

Norwegian University  
of Life Sciences

**Master's Thesis 2019 60 ECTS**

Faculty of Environmental Sciences and Natural Resource Management

# **Rainfall-runoff modelling with high temporal resolution on the arable catchment Skuterud**

- Assessing the performance of the Distance Distribution Dynamics model**

Anne Ellekjær Stavang

Environment and Natural Resources



# Acknowledgement

This thesis is written as the final part of a master's degree in Environment and Natural Resources at the Faculty of Environmental Sciences and Natural Resource Management (MINA) at the Norwegian University of Life Sciences (NMBU).

I would like to thank a selected few who have given influential support to my thesis. Firstly, my supervisor Nils-Otto Kitterød for helpful feedback and valuable advice throughout the thesis process. Secondly, Thomas Skaugen at NVE for his help with the model setup and motivating discussions. Further, I want to acknowledge Ståle Haaland for his feedback and comments on the thesis structure and discussion. The involvement and assistance of Johannes Deelstra and the JOVA programme is greatly appreciated. Tormod Solem and Follo Landbrukskontor also deserves acknowledgment for helping me investigate the layout and extent of the artificial drainage system in Skuterud catchment.

To my parents, thank you for encouragement and support throughout my study. A special thanks to my sisters for proofreading.

Norwegian University of Life Sciences (NMBU)

Ås, 14.05.2019

Anne Ellekjær Stavang



# Abstract

Runoff from arable land is recognised as the main reason for water degradation, eutrophication and reduced water quality. The aim of the study is to model runoff on a 1h temporal resolution from an arable catchment using the Distance Distribution Dynamics model. Research objectives are to compare the model with and without artificial drainage system as part of the model parameters and introduce two alterations to the recession analysis of the pre-processing routine. Model inputs are precipitation and temperature. Pre-processing includes recession analysis, to determine subsurface storage and subsurface flow velocities i.e. celerities, and distance distribution analysis. The study area is the small agriculturally dominated catchment Skuterud, which is a part of The Norwegian Agricultural Environmental Monitoring Programme (JOVA). The calibration period is from 2000-2004, and the validation period 2005-2009. Time series from 2000-2004 were aggregated to 3h, 6h, 12h and 24h temporal resolution to check the assumption of time invariance for the recession characteristics. The results show an improvement of Nash-Sutcliffe efficiency (NSE) and Kling-Gupta Efficiency (KGE) criterion when artificial drainage is included in the model, and further improvement using the altered recession analysis methods. Limitation and uncertainties with the model include, but is not limited to, instrumental limitation for runoff measurements at low flow, hydrological impact on soil characteristics or seasonal influences. The overall best result is an NSE of 0.56 and KGE of 0.74.



# Sammendrag

Avrenning fra jordbruksdominerte nedbørfelt er en av hovedkildene til vannforurensing og eutrofiering i omkringliggende innsjøer og elver. Målet med dette studiet er å modellere avrenning fra et jordbruksfelt ved hjelp av *Distance Distribution Dynamics* (DDD) modellen på 1t tidsoppløsning. Delmål inkluderer implementering av drenerør i avstandsfordelingsrutinen og endringer i resesjonsanalysen som brukes til å estimere vannets bølgehastighet gjennom bakken. Inndata er nedbør og temperatur, parameterdata estimeres i avstandsfordeling- og resesjonsanalyse. Fokusområdet for oppgaven er Skuterud nedbørfelt som er et av forskningsfeltene til *Jord- og vannovervåking i landbruket* (JOVA). Fire ulike modellscenarier kalibreres i perioden 2000-2004 og valideres i perioden 2005-2009. Resultatene viser akseptable ( $> 0.5$ ) Nash-Sutcliffe (NSE) og Kling-Gupta (KGE) kriterier for simulering på 1t tidsoppløsning. Simuleringen bedres ved implementering av drenerør i modellens avstandsfordeling. Endringene i resesjonsanalysen bedrer resultatene, men ikke i like stor grad. Dette kan skyldes begrensninger ved hydrologisk måling når vannstanden er lav, og hydrologiske eller sesongvariasjoners påvirkning på jordegenskaper. Det beste resultatet er en NSE på 0.56 og en KGE på 0.74.



# Table of contents

Acknowledgement.....	i
Abstract .....	iii
Sammendrag.....	v
Introduction .....	1
1.1. Motivation .....	1
1.2. Research focus & literature review .....	3
1.3. Research objectives .....	5
1.4. Outline .....	6
Methods & Materials.....	7
2.1. The Distance Distribution Dynamics model .....	7
2.2. Evaluation criterion .....	18
2.3. Study area .....	21
2.4. Tools .....	23
2.5. Model setup .....	24
Results .....	31
3.1. Distance distribution.....	32
3.2. Recession analysis .....	36
3.3. Calibration and validation of model scenarios .....	45
Discussion .....	53
4.1. Distance distribution.....	53
4.2. Recession analysis .....	54
4.3. Calibration and validation of model scenarios .....	64

Conclusion.....71

5.1. Aim and research objectives .....71

5.2. Reflections and further studies .....71

References .....73

# Introduction

## 1.1. Motivation

### 1.1.1. Runoff, water quality and climate change

Runoff from arable land is recognised as a main reason of water degradation, eutrophication and reduced water quality (Deelstra et al., 2011; Vagstad & Bechmann, 2013). Runoff is the amount of water from precipitation that travels on the surface and subsurface through the catchment to lakes and rivers. It is composed of direct runoff; the contribution from overland flow and quick interflow, and base flow; the contribution from delayed interflow and groundwater runoff (Ramirez, 2000). The process of runoff generation is complex: It depends on the climate, shape, size, topography, geology, soil and storage characteristics of the catchment. The runoff process can carry high amounts of organic and inorganic matter, pesticides, nutrients or pollutant from the catchment to lakes and rivers. Consequently, the runoff process closely relates to water pollution.

Water pollution is the introduction of a substance that weakens the quality of the aquatic ecosystem. It is introduced through the air, soil or water, and has indirect or direct effect on the water body (Union, 2000). Specifically, anthropogenic water pollution is a result of contamination of substances from human activity. Sources include, but are not limited to, acid rain, agriculture, mining, urbanization and runoff from sewage and roads. These substances can come from one specific source (point source) or many diffuse sources (non-point) and can be both local and long transported. Water pollution has a harmful effect on the biogeochemistry of fresh water systems and negatively affect the organisms living in and off the water (Smol, 2008). A common consequence of anthropogenic pollution is enhanced eutrophication. Eutrophication is an increase in primary production and trophic state due to enrichment of nutrients. Typical signs of eutrophication are the occurrence of algal blooms and changes in macrophytes and oxygen levels. The algal blooms are often toxic, and make water unfit for recreational purposes and unviable as a source of drinking water (Romarheim & Riise, 2009). Changes in oxygen level and macrophytes might damage other organisms living in the water. The most important, and often limited, nutrients for primary production is phosphorus and nitrogen.

Agricultural lands are dominated by soils rich in phosphorus and nitrogen due to fertilizing. The phosphorus and nitrogen are main sources of nutrient load to the environment. The rate of nutrient loss from agricultural catchments is determined by runoff rates, farming practices, soil types, topography and climate conditions (Deelstra et al., 2011). Scenarios of the global climate up to 2100 indicates an increase in runoff rates for Norway (Deelstra et al., 2011). The Norwegian climate is presumed to have less snow accumulation, more frequent winter floods and fewer spring floods, more autumn precipitation, and more extreme events such as floods and droughts (Klimaservicesenter). A changing climate will lead to change in runoff patterns, which in turn will affect nutrient load to the aquatic ecosystems. The European Union (EU) Water Framework Directive (WFD) was established in 2000 to provide guidelines for assessment, management, protection and improvement of the quality of water across EU (Union, 2000). One of the main goals of the directive is that waters must achieve good ecological and chemical status, to protect human health, water supply, natural ecosystems and biodiversity (Union, 2000). In order to accomplish the goal, set by the Water Framework Directive, the study of rainfall-runoff processes from agricultural catchment needs to be further researched.

### 1.1.2. Rainfall-runoff modelling

One approach to the study of rainfall-runoff processes is through rainfall-runoff models. Runoff generation is a complex process and we do not have the means to measure all parts of the hydrological process. Rainfall-runoff modelling estimates processes of the real world based on a theoretical or mathematical approach using fewer measurements (Beven, 2012). This can be helpful for investigating sites that do not have measurement, and future climate change scenarios. If we can determine what controls runoff patterns today it can help gain insight to the changes that will happen in the future. This will help prepare mitigation and abatement measurements to minimise the negative effects of climate change and changing runoff patterns has on the aquatic ecosystem.

There are many different approaches to rainfall-runoff modelling. Physical models reproduce the natural world at a larger or smaller scale, analogue models use knowledge of one physical process to simulate a physically analogue natural process, and mathematical models use algorithms, logical steps and equations based on theory to simulate natural processes (Dingman, 2015). Mathematical models have different approaches to how runoff is calculated (Sitterson et al., 2017). Physically based models describe the hydrologic processes using physical laws (Dingman, 2015; Sitterson et

al., 2017). Conceptual models use simple transfer function to minimise the number of calibrated parameters (Dingman, 2015). There are also different approaches to spatial and temporal representation (Dingman, 2015). The spatial representation is either lumped or distributed. Lumped models treat the catchment as a single unit and represent the catchment characteristics using an average (Beven, 2012). Distributed models divide the catchment into zones or grids. Each grid is represented by an average (Beven, 2012). The semi-distributed models aim to fit a distribution function of characteristics to the catchment and make all calculations based on the function (Beven, 2012). Temporal representation is either steady-state, single-event or continuous (Dingman, 2015). Steady-state models focus on the long-term average or equilibrium, single-event models simulate isolated events and continuous models simulate sequence of responses (Dingman, 2015). In order to choose the right model, it is important to consider the main objective of the modelling and try to determine if the model of choice has the right output to answer the research question.

## **1.2. Research focus & literature review**

The research focus of this study is to model runoff using a rainfall-runoff model at high temporal resolution (1h) on an arable catchment. Deelstra and Iital (2008) found that diurnal variation is important when considering nutrient loss processes from agricultural catchments. Simulations of runoff patterns at high temporal resolution represent the diurnal variations and extreme events of the catchments and is important in order to understand the hydrological processes governing in the catchment (Deelstra et al., 2010). Modelling runoff from an arable catchment is challenging. A common mitigation to deal with water logging and increase productivity in agriculturally dominated lands is to install artificial drainage (Hauge et al., 2011). Artificial drainage enhances the productivity of crops, but alter the total annual water flow and change the natural water balance of the catchment (Gramlich et al., 2018). Other anthropogenic influences on the water balance include irrigation, urban areas and sewage. It is thus important to consider that runoff processes in these catchments might differ from natural catchments.

The Norwegian Agricultural Environmental Monitoring Programme (JOVA) has worked on documenting the environmental effects of agriculture on water quality since 1992 (Bechmann & Deelstra, 2013; JOVA, 2019). One of their monitored catchments is the Skuterud catchment. Skuterud is a small, agriculturally dominated catchment in the southeast of Norway. Farkas et al.

(2016) conducted a study comparing five rainfall-runoff models' ability to predict runoff from Skuterud. The models were SWAT, COUP, DRAINMOD, HBV and INCA. DRAINMOD and COUP are one-dimensional, physically based models. DRAINMOD was developed to model the hydrology of poorly and/or artificially drained soils, and to predict the effects of drainage and water management practices on water table depths (Skaggs et al., 2012). COUP focuses on the vertical movement of water, heat, carbon, nitrogen and solutes in the soil profile (Jansson & Karlberg, 2004). HBV, INCA and SWAT are semi-distributed catchment models describing the surface and subsurface runoff generation process in an integrated way. HBV simulates the characteristics of the rainfall-runoff process and calculates the water balance for 10 elevation zones (Lindström et al., 1997). INCA describes water and mass transport in the soil and stream system, and was first introduced by Jarritt and Lawrence (2006). SWAT quantifies the impact of land management practices in large watersheds on water supply and nonpoint pollution (Arnold et al., 1998). The five models were tested on one year, one month, one week and one day temporal resolution. The study had two relevant conclusions. First, the models performed well on yearly, monthly and weekly basis, but unsatisfactory on daily temporal resolution (Farkas et al., 2016). Secondly, the more complex models, with more calibrated parameters, did not necessarily perform better than simpler models (Farkas et al., 2016).

Using many calibrated variables makes it difficult to find what the errors of the model are, and in which process representation they lie. Calibrated parameters are optimised for a specific catchment for a specific period. This makes them unsuitable for future prediction. Skaugen & Onof (2014) at the Norwegian Water Resource and Energy Directorate first authored the DDD model. It is operational at 3h and 24h temporal resolution for flood forecasting services (Skaugen & Onof, 2014). The development of the DDD-model was initiated with the advance of new technology. The use of satellites and GIS has provided detailed observations of catchments and its characteristics, and the idea was that parameters should be derived from these observations and actual measurements, not calibrations. In the DDD model parameters derive from the *distance distribution* of points in catchment to river reach and points in river network to river outlet, and *recession analysis* based solely on the runoff measurements. The distance distribution is used to describe how the catchment is drained, and the recession analysis adds velocities and moisture states of the subsurface. Skaugen and Onof (2014) compared the DDD model with the HBV model and found that DDD predicts floods more precisely in both timing and amount. It shows a better representation

of the groundwater and subsurface water description, even with less calibrated parameters. The model has been developed and tested for 140 Norwegian catchments (Skaugen & Onof, 2014; Skaugen et al., 2015; Skaugen & Saloranta, 2015; Skaugen & Mengistu, 2016; Skaugen & Weltzien, 2016), but not for agriculturally developed land.

### 1.3. Research objectives

The aim of this study is to model runoff from an agricultural catchment on 1h temporal resolution. The research objectives and corresponding hypotheses are as follows:

- To provide a rainfall-runoff model that satisfactorily simulate runoff on 1h temporal resolution.

*Hypothesis:* Due to good simulation of the subsurface and few calibrated parameters, the DDD model will perform better than previous models and provide a satisfactory estimation of runoff patterns on an hourly temporal resolution.

- To implement the artificial drainage system as river network in the model and assess the effect on the modelling results.

*Hypothesis:* When adding artificial drainage network as river network the model improves its overall runoff simulation and peak flow estimation.

- To improve the recession analysis for the subsurface celerity estimation. The main goal of the two altered estimation methods are to filter out erroneous observations that are most likely a result of high temporal resolution, measuring error or runoff variability.

*Hypothesis:* Using the parameters of the altered recession methods will yield better calibration and validation results than the original method.

## 1.4. Outline

This thesis will model runoff using the Distance Distribution Dynamics model in order to provide a rainfall-runoff model that satisfactorily simulate runoff on 1h temporal resolution from the agricultural catchment, Skuterud.

In order to understand, compare and discuss the results of the model, the DDD model background, theory and parameter data are introduced first. To make results comparable to other studies, the evaluation criterion and how to objectively interpret the results will be stated. Study area, tools, pre-processing routine, data acquisition and the four model scenarios needed to complete the modelling are included in the materials section. The results of the pre-processing routine of distance distribution and recession analysis are stated to highlight the differences in input parameter data of the different model scenarios. The main results of the calibration and validation are presented last. Main discussion topics are the effect of including the artificial drainage network, the effect of altering the recession analysis, and lastly a discussion of the best model scenario.

# Methods & Materials

## Method

### 2.1. The Distance Distribution Dynamics model

The DDD model is written in the programming language R (see 2.4 Tools). The model simulates saturated soil water flow, states of subsurface, snow accumulation, distribution and melt, and runoff for a given catchment. Model inputs are measurements of temperature and precipitation. Parameter data are estimated from observations.

#### 2.1.1. Background

The DDD model is an extension of the unit hydrograph method (Skaugen & Onof, 2014). The unit hydrograph (UH) of a watershed is defined as the direct runoff hydrograph resulting from one unit volume (1 mm or 1 in) of excess rainfall at a constant intensity and uniformly distributed over the drainage area for a duration of time (Dooge, 1959; Ramirez, 2000; Sherman, 1932). The duration of the UH, or response time, is the time it takes for the water farthest away in the catchment to reach the outlet. The UH is derived from the relationship between the hydrograph and catchment area. The hydrograph is the runoff measured at a point in the river, usually the outlet, over time. The shape and size of the hydrograph are determined by *catchment characteristics*: shape, size, slope, elevation, drainage density, *infiltration characteristics*: land use and cover, soil type and geology, the occurrence of lakes and swamps and *river network characteristics*: cross-section, roughness and storage capacity (Subramanya, 2013). The UH of a catchment is thus a reflection of the individual catchment and its response to one unit of rainfall excess. In discretised form, the ordinates of the UH is used to estimate the direct runoff of any storm of any length (Sherman, 1932; Skaugen & Onof, 2014).

There are two main assumptions that constitute the basis of the unit hydrograph theory. The first is time invariance, which implies that the UH is the same for any rainfall event in time (Dooge, 1959; Subramanya, 2013). The second assumption is a linear response, which assumes a linear relationship between the runoff response to a given rainfall excess. This implies scaled responses

for rainfall events of different intensity, and superimposed responses of several rainfall events. If three rainfall excess events occur consecutively, their combined effect is obtained by superposing the respective UHs (Dooge, 1959; Ramirez, 2000; Subramanya, 2013).

### 2.1.2. Modules

The DDD model consists of two parts, the hydrological module and the runoff dynamics module (Skaugen & Onof, 2014). The hydrological module estimates the amount of excess water that enters the runoff dynamics module. The runoff dynamics module use distance distribution analysis to describe the transport of water from hillslope to river network and from river network to outlet. In addition, recession analysis is used to provides celerities of water transport. The two parts create the UH of the hillslope and the UH of the river network. The combination of the two UHs estimates how an impulse of water is temporally and spatially distributed through the hillslope and river network (Skaugen & Onof, 2014).

#### Hydrologic module

The excess water for a single time step is estimated in the hydrologic module of the DDD model, illustrated in Figure 1.  $I(t)$  is the input of precipitation and snow,  $E_a(t)$  is the actual evapotranspiration,  $Z(t)$  is the soil water content of the total volume  $D(t)$  of the unsaturated zone, and  $S_s(t)$  is the volume and water content of the saturated zone.  $M$  is the shared volume of  $D(t)$  and  $S_s(t)$ , and thus the total volume of the subsurface reservoir.  $X(t)$  is the excess water reservoir of the unsaturated zone, and  $Q(t)$  is the excess water from the saturated zone (Skaugen & Onof, 2014).

Precipitation is distributed to 10 elevation zones in the catchment. To distinguish between precipitation as rain or snow a temperature threshold,  $TX = 0.5$  °C, is used,

$$\text{If } T > TX, \quad P_{rain} = P \cdot \theta_{precip} \quad (1)$$

$$P_{snow} = 0.0$$

$$\text{If } T < TX, \quad P_{snow} = P \cdot \theta_{snow} \quad (2)$$

$$P_{rain} = 0.0$$

Where  $T$  is the observed temperature,  $TX$  is the temperature threshold,  $P$  is the total precipitation,  $P_{rain}$  is precipitation as rain,  $P_{snow}$  is precipitation as snow,  $\theta_{precip}$  is the precipitation correction factor

used if temperature is greater than 0.5 °C (equation 1), and  $\theta_{snow}$  is the snow correction used when temperature is below 0.5 °C (equation 2).

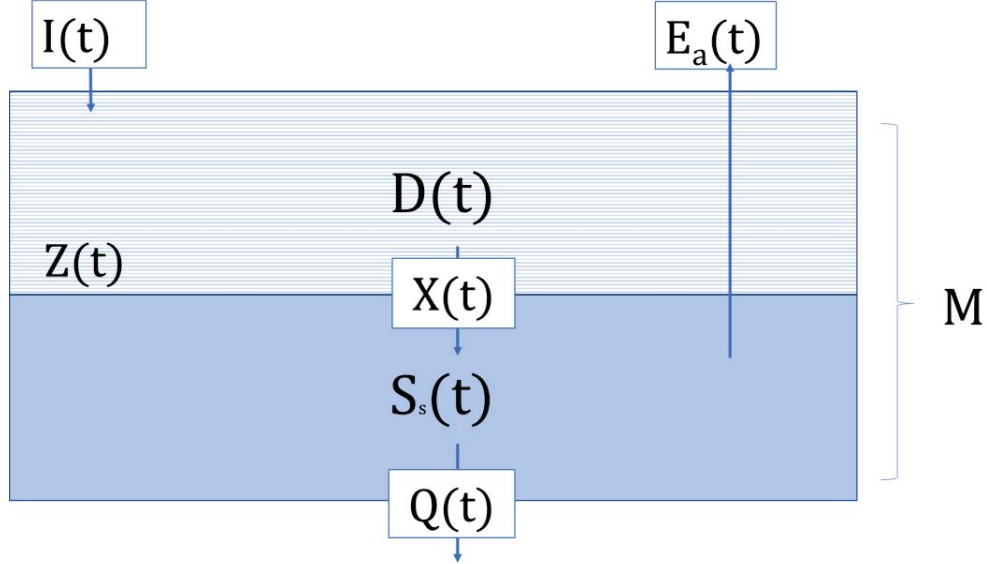


Figure 1 Illustration of the hydrologic module of the DDD model. Edited from Skagen and Onof, 2014.

The input of water can, in addition to precipitation, come from snowmelt. To estimate the amount of melt equation 3 is used

$$\Delta SWE = \frac{K + L_{net} + H + LE + G + R - CC}{(\lambda_F \rho_w)} \quad (3)$$

Where  $\Delta SWE$  [m] is the change in snowpack's water equivalent,  $K$  [ $\text{kJm}^{-2}$ ] is net shortwave radiation,  $L_{net}$  [ $\text{kJm}^{-2}$ ] is the atmospheric and terrestrial net longwave radiation,  $H$  [ $\text{kJm}^{-2}$ ] is the sensible heat exchange,  $LE$  [ $\text{kJm}^{-2}$ ] is the energy flux related to vaporisation and condensation of water vapor,  $G$  [ $\text{kJm}^{-2}$ ] and  $R$  [ $\text{kJm}^{-2}$ ] is the ground and precipitation heat and  $CC$  [ $\text{kJm}^{-2}$ ] is snowpack heat storage.  $\lambda_F$  [ $\text{kJkg}^{-1}$ ] is latent heat fusion and  $\rho_w$  [ $1000\text{kgm}^{-3}$ ] is the density of water. These values are estimated as a function of location, time of year, precipitation and air temperature (Skaugen & Saloranta, 2015).

The energy balance is used for estimating the potential evapotranspiration,  $E_p$ . The DDD model use the Priestly-Taylor method for estimating potential evapotranspiration (Priestley & Taylor, 1972)

$$E_p(t) = \alpha_{PT} * \left( \frac{\delta}{\delta + \gamma} \right) * (K + L_{net}) * \left( \frac{1000}{LE * \rho_w} \right) \quad (4)$$

Where  $\alpha_{PT}$  is the Priestly-Taylor constant,  $\delta$  is the slope of saturation vapor pressure-temperature relation [P T],  $\gamma$  is the psychrometric constant [P T<sup>-1</sup>], K [kJm<sup>-2</sup>] is net shortwave radiation,  $L_{net}$  [kJm<sup>-2</sup>] is the atmospheric and terrestrial net longwave radiation, LE [kJm<sup>-2</sup>] is the energy flux related to vaporization and condensation of water vapor and  $\rho_w$  [1000kgm<sup>-3</sup>] is the density of water. The actual evapotranspiration,  $E_a$ , is a function of  $E_p$  and the combined water content of the saturated  $S_s(t)$  and unsaturated  $Z(t)$  reservoirs.

$$E_a(t) = E_p(t) * ((S_s(t) + Z(t))/M) \quad (5)$$

When the input,  $I(t)$ , reaches the unsaturated zone,  $D(t)$ , it adds to the volume  $Z(t)$ . Movement of water from  $D(t)$  to  $S_s(t)$  happens when the actual water content,  $Z(t)$ , reaches field capacity,  $R_{fc}$ , of 0.3 which is of 30 % of the capacity of  $D(t)$ . The change in soil water content is,

$$\frac{dZ}{dt} = I(t) - X(t) \quad (6)$$

Where  $X(t)$  is the excess water volume to saturated zone  $S_s(t)$  and is the amount of water that exceeds 30 % of the volume of  $D(t)$ .

$$X(t) = Max \left\{ \frac{I(t) + Z(t)}{D(t)} - R, 0 \right\} D(t) \quad (7)$$

The volume  $X(t)$  is added to the volume of the saturated zone  $S_s(t)$  where  $Q(t)$  is the water output from the saturated zone, and the change in  $S_s(t)$  is

$$\frac{dS_s}{dt} = X(t) - Q(t) - E_a(t) \quad (8)$$

## The runoff dynamics module

To estimate direct runoff  $Q(t)$  at the outlet, the convolution integral of excess water from hillslope  $Q_h(t)$  and the unit hydrograph  $u_r$  of the river network, is used

$$Q(t) = \int_0^t Q_h(\tau)u_r(t - \tau)d\tau \quad (9)$$

where  $Q_h$  is the excess water contributed by the hillslope. It is estimated using the convolution integral of excess water  $X(\tau)$  (from the hydrologic module) and the unit hydrograph  $u_h$  of the hillslope.

$$Q_h(t) = \int_0^t X(\tau)u_h(t - \tau)d\tau \quad (10)$$

### Deriving the unit hydrograph for hillslope

The unit hydrograph is derived from distance distribution and recession analysis. The distance distribution is the cumulative distribution of actual distances (m) from points in the catchment to the river network. The distribution is modelled as an exponential distribution with a cumulative distribution function (CDF) illustrated in Figure 2 and equation 11.

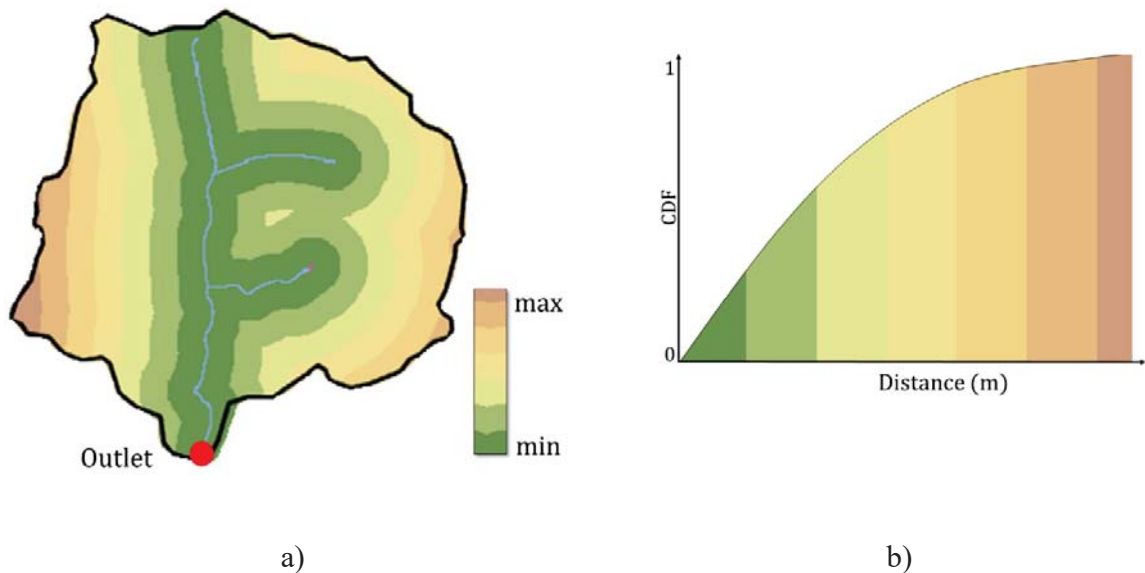


Figure 2 (a) An illustration of the distribution of distances (m) from river network in a catchment and (b) the corresponding CDF of distances (m).

$$U_h(d) = 1 - e^{-\Lambda(d-d_0)} \quad (11)$$

$\Lambda$  is the rate constant of the exponential distribution. If water transport down the hillslope is constant with velocity  $v_h$ , then  $\Delta d$  is the distance travelled by water during the time step  $\Delta t$  (Skaugen & Onof, 2014). The distance distribution is then a distribution of travel times where the response time  $t_{h,max} = d_{max}/v_h$ .

$$U_h(t) = 1 - e^{-\Lambda(t-t_0)} \quad (12)$$

The derivative of  $U_h$  is the unit hydrograph of the hillslope,  $u_h$ , where  $\Lambda$  is the parameter used to describe its characteristics. The velocity  $v_h$  and  $\Lambda$  are estimated through recession analysis. The  $u_h$  of the hillslope is then

$$u_h(t) = \Lambda e^{-\Lambda(t-t_0)} \quad (13)$$

### Deriving the unit hydrograph for each subsurface saturation level

The DDD model assumes different levels,  $i = 1 \dots I$ , of saturation based on the distribution of  $\Lambda$ . The saturation levels have different velocities and recession characteristics. The level specific unit hydrograph is

$$u_{h,i}(t) = \lambda_i e^{-\lambda_i(t-t_0)} \quad (14)$$

Where  $\lambda_i$  is the level specific recession characteristic. The  $u_{h,i}$  is further discretised into intervals,  $j_i = 1 \dots J_i$ , to obtain the weights  $\mu_{i,j}$  that each layer contributes at each time interval. The number of intervals for each level is  $J_i = t_{h,i,max}/\Delta t$ . Where  $t_{h,i,max} = d_{max}/v(i)_h$ .  $d_{max}$  is the maximum distance observed in the distance distribution and  $v(i)_h$  the level specific celerity estimated from recession analysis. The number of time intervals  $J_i$  is the time it takes for the wave farthest away in the hillslope to reach the river network. The weight of each time interval  $j$  at level  $i$  (equation 15) is illustrated in Figure 3.

$$\mu_{i,j} = \int_{(j-1)\Delta t}^{(j)\Delta t} u_{h,i}(t) dt \quad j = 1 \dots J_i \quad \sum \mu_{i,j} = 1 \quad (15)$$

The runoff from each interval and saturation level is then,

$$Q_h(j\Delta t) = \frac{1}{I} \sum_{i=1}^I X(\Delta t) \xi_{i,j} \mu_{i,j} \quad (16)$$

Where  $\xi_{i,j}$  is the weights distributing  $X(\Delta t)$  to each saturation level  $i$  and interval  $j$  depending on their individual degree of saturation.

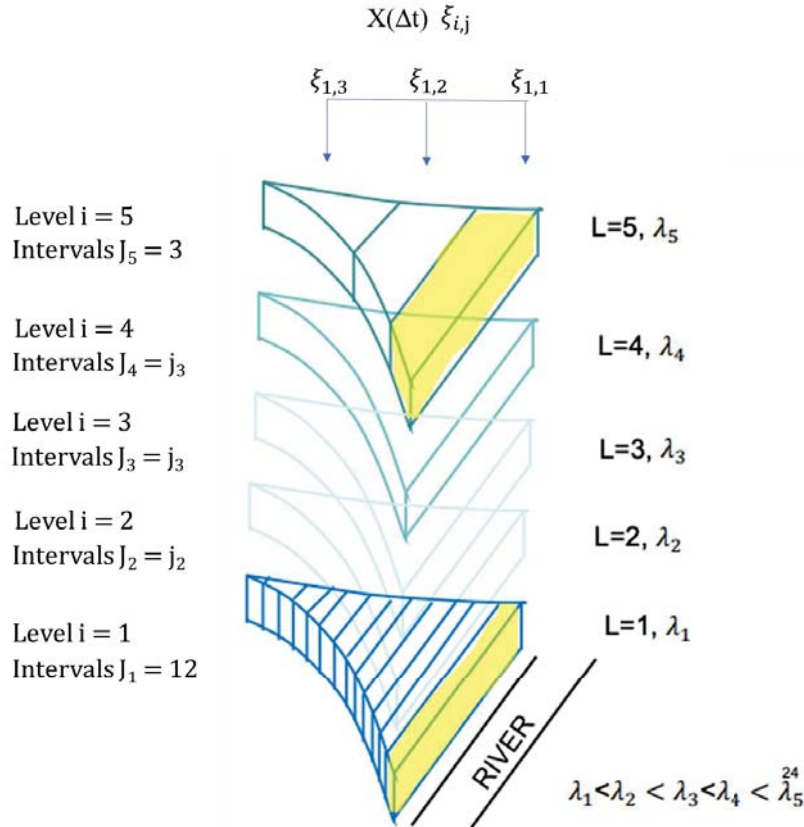


Figure 3 Illustration of the subsurface saturation levels  $i = 1 \dots 5$ , where each has its own UH defined by the recession characteristic  $\lambda_i$  and individual no. of intervals  $J_i = 1 \dots J_i$ . Edited from Skaugen (2018).

### Estimating the level specific celerity using recession analysis

In the DDD model, recession analysis is used to assign celerities to the superimposed UHs and determine the distribution of saturation levels. Recession analysis is the study of how a catchment drains after a rainfall episode. The method investigates the recession period of the hydrograph, which is the part of the hydrograph after the peak flow when flow decreases. The assumption is that the recession period reflects the withdrawal of water from the storage reservoirs in the

catchment and that there is a direct link between subsurface storage and runoff recession. The relationship between change in storage and runoff is often modelled as a power law relationship (Brodie & Hostetler, 2005; Kirchner, 2009; Stoelzle et al., 2013), and its shape and size say something about the contributing storage reservoirs (Subramanya, 2013). The recession characteristic is individual for each catchment and aims to provide information about the storages that convey water to the outlet (Skaugen & Onof, 2014; Tallaksen, 1995). The DDD model models the rate of the recession curve using the following equation

$$Q(t) = Q_0 \Lambda e^{-\Lambda(t-t_0)} \quad (17)$$

$Q_0$  is the discharge at the start of the recession period.  $\Lambda$  is the slope of the recession curve and determined from the log-difference in discharge at time  $t$  during the recession (equation 18). A high  $\Lambda$  indicates a large change in storage and subsequent higher celerity  $v_h$  (equation 19).

$$\Lambda(t) = \log Q(t) - \log Q(t + \Delta t) \quad (18)$$

$$v_h = \frac{\Lambda \bar{d}}{\Delta t} \quad (19)$$

The parameter  $\bar{d}$  is the mean of the distance distribution, and  $\Lambda$  is the slope of the recession. There are different celerities  $v_h$  corresponding to different saturation levels  $i$ . The celerity for each level is estimated as

$$v(i)_h = \frac{\lambda_i \bar{d}}{\Delta t} \quad (20)$$

Where  $\lambda_i$  is the level specific recession characteristic and is solved using the assumption that  $\lambda_1 = \Lambda_1$

$$\Lambda_i e^{-\Lambda_i(t-t_0)} = w_1 \lambda_1 e^{-\lambda_1(t-t_0)} + w_2 \lambda_2 e^{-\lambda_2(t-t_0)} + \dots + w_{i+1} \lambda_{i+1} e^{-\lambda_{i+1}(t-t_0)} \quad (21)$$

$\Lambda_i(t - t_0)$  is integrated over all saturation levels for the hillslope. The weights  $w_i$  reflect the discharge each level of saturation contributes and is estimated

$$w_i = \frac{\Lambda_i}{\sum_{k=1}^i \Lambda_k} \quad (22)$$

### Distribution of saturation level and estimation of the mean storage

The DDD assumes that the variability in celerity for each level is due to the variability in storage and the higher the saturation level is, the higher the celerity. This is reflected by a higher difference in subsequent runoff values in equation 18 (Skaugen & Onof, 2014). The distribution of  $\Lambda$  is modelled as a gamma distribution (Equation 23). This distribution reflects the distribution of saturation, so that the saturation levels are also modelled as a gamma distribution (Equation 24),

$$f(\Lambda) = \frac{1}{\beta^\alpha \Gamma(\alpha)} \Lambda^{\alpha-1} e^{-\frac{\Lambda}{\beta}}, \quad \alpha > 0, \quad \beta > 0 \quad (23)$$

where  $\alpha$  is the shape parameter and  $\beta$  is the scale parameter of the gamma distribution. The expected mean value  $E(\Lambda)$  is  $\alpha\beta$  and variance  $\text{Var}(\Lambda)$  is  $\alpha\beta^2$

$$f(S_s) = \frac{1}{\eta^\alpha \Gamma(\alpha)} S_s^{\alpha-1} e^{-\frac{S_s}{\eta}}, \quad \alpha > 0 \quad \eta > 0 \quad (24)$$

Where the  $\eta = \beta/c$ , and  $c = \bar{\Lambda}/m_s$ .  $\alpha$  is the shape parameter,  $\eta$  is the scale parameter and  $m_s$  is the mean storage. The mean storage  $m_s$  is estimated through the daily excess moisture input  $X$ , which depends on the mean annual runoff (MAR) and catchment area ( $A$ )

$$X[\text{mm day}^{-1}] = \frac{(1000 \cdot \text{MAR}[\text{m}^3 \text{s}^{-1}] \cdot 86400 [\text{s}])}{A[\text{m}^2]} \quad (25)$$

The total sum of moisture input  $X$  after  $J$  days is

$$J \cdot X = S_{ss} + Q_{ss} \quad (26)$$

Where  $Q_{ss}$  is the total runoff after  $J$  days,  $S_{ss}$  is the water left in the soil and represent the mean storage  $m_s$

$$Q_{ss} = \sum_{k=1}^J \sum_{j=1}^k X \cdot \mu(\bar{\Lambda})_j \quad (27)$$

$$S_{ss} = \sum_{k=1}^{J-1} \sum_{j=k+1}^J X \cdot \mu(\bar{\Lambda})_j \quad (28)$$

The distribution of each level  $S_i$  is then calculated as quantiles of  $f(S)$  where the subsurface reservoir capacity,  $M$ , is the 99 % quantile of the distribution of  $S$ .

$$\frac{S_i}{M} = \int_0^{S_i} \frac{1}{\eta^\alpha \Gamma(\alpha)} S S^{\alpha-1} e^{\left(-\frac{S}{\eta}\right)} dS \quad (29)$$

### Deriving the unit hydrograph of the river network

The same principles apply when deriving the river network  $u_r$ . The distance distribution of points in river network to the outlet is determined as the distance from points in the river network to the outlet. The mean celerity of the river network  $v_r$  is used to transform the function to a distribution of travel times. The unit hydrograph of the river,  $u_r$ , is the derivative of the cumulative distribution function of travel times where  $t_{r,max} = R_{d,max}/v_r$ .  $R_{d,max}$  is the maximum distance from points in the river network to outlet,

$$U_r(t) = \int_0^t u_r(t) dt, \quad U_r(t_{r,max}) = 1 \quad (30)$$

### 2.1.3. Input and model parameters

Input data in the DDD model is precipitation and temperature. Model parameters include estimations from GIS analysis and recession analysis, calibrations and fixed values. Input data in the GIS analysis include digital elevation maps to estimate the hypsographic curve, and river network and area cover database, to estimate the distance distribution. Recession analysis is based on discharge measurements from the catchment. All model parameters (estimations, calibrations and fixed values) are listed in Table 1.

Additional parameters include glacier fraction, the mean and standard deviation of distance distribution for glacier and the areal fraction of glaciers in the elevation zone. These are not relevant for Skuterud and not listed in the table.

Table 1 Parameter data of the DDD model for Skuterud with description and method of estimation.

<b>Parameter</b>	<b>Description</b>	<b>Method of estimation</b>
<b>Hypsographic curve</b>	11 values describing the quantiles of the elevation.	GIS
$\theta_{ws}$ (%)	Max liquid water content in snow	Observation
<b>Hfelt</b>	Mean elevation of catchment	GIS
$\theta_{Precipitation}$	Correction factor for precipitation	Calibrated
$\theta_{Snow}$	Correction factor for precipitation as snow	Calibrated
$\theta_{TX}$ (°C)	Threshold temperature rain/snow	Fixed, 0.5
$\theta_{TS}$ (°C)	Threshold temperature melting/freezing	Fixed, 0.0
<b>CFR (mm °C<sup>-1</sup> hr<sup>-1</sup>)</b>	Degree-day factor for freezing	Fixed, 0.02
<b>Area (m<sup>2</sup>)</b>	Catchment area	GIS
<b>d<sub>max,bog</sub> (m)</b>	Max distance for bogs	GIS
<b><math>\bar{d}_{bog}</math> (m)</b>	Mean distance bogs	GIS
<b>Frac</b>	Fraction of bogs in catchment	GIS
<b>Z<sub>soil</sub></b>	Area fraction of zero distance for soil	GIS
<b>Z<sub>bog</sub></b>	Area fraction of zero distance for bogs	GIS
<b>NOL</b>	Number of storage layers	5
<b>R</b>	Ratio defining field capacity	0.3
<b><math>\alpha</math></b>	Shape parameter of gamma distributed celerities	Recession analysis
<b><math>\beta</math></b>	Scale parameter of gamma distributed celerities	Recession analysis
<b><math>\theta_{CV}</math> (m s<sup>-1</sup>)</b>	Coefficient of variation for spatial distribution of snow	Observations
<b>a0</b>	Par for new spatial dist of SWE, shape parameter	Estimated from precip.
<b>D</b>	Decorrelation length of spatial precipitation.	Estimated from precip.
<b><math>\theta_{vr}</math> (m/s)</b>	Mean celerity in river	Calibrated
<b><math>\bar{d}_{river}</math> (m)</b>	Mean distance of river network	GIS
<b>SD<sub>river</sub> (m)</b>	Standard deviation of distance distribution of river	GIS
<b>d<sub>max,river</sub> (m)</b>	Max of distance distribution of the river	GIS
<b><math>\bar{d}_{soils}</math> (m)</b>	Mean of distance distribution soil	GIS
<b>d<sub>max, soils</sub></b>	Max of distance distribution for soil	GIS

## 2.2. Evaluation criterion

A rainfall-runoff model provides an estimation of the real world. To evaluate how good the estimate is, the “goodness-of-fit” must be evaluated as objectively as possible. In this study, the model output is assessed with the Nash-Sutcliffe efficiency criterion (Nash & Sutcliffe, 1970) and the Kling-Gupta efficiency criterion (Kling & Gupta, 2009).

The Nash-Sutcliffe efficiency criterion (NSE) is a dimensionless skill score ranging from  $-\infty$  to 1.0, where an NSE of one indicates a perfect fit. The NSE value is obtained by dividing the mean square error (MSE), which is the difference between the simulated discharge and observed discharge, by the variance of the observations and subtracting the result from 1.0 (Equation 31),

$$NSE = 1 - \frac{\sum_{t=1}^T (Q_s^t - Q_o^t)^2}{\sum_{t=1}^T (Q_o^t - \overline{Q_o})^2} \quad (31)$$

where  $Q_s^t$  is the simulated discharge,  $Q_o^t$  the observed discharge and  $\overline{Q_o}$  is the mean of observed discharge. The NSE value represents how much of the observed variance is explained by the models mean squared error (Ritter & Muñoz-Carpena, 2013). The main drawback with using NSE as a skill score is that it uses the observed mean as a reference. This can cause an overestimation of model skill score for seasonal variables (i.e. snowmelt) and outliers (i.e. extreme events) (Gupta et al., 2009; Ritter & Muñoz-Carpena, 2013). Gupta et al (2009) proposed a revised NSE to deal with the problem of overestimation and bias, and named it the Kling-Gupta Efficiency criterion (KGE),

$$KGE = 1 - \sqrt{(r - 1)^2 + (v - 1)^2 + (z - 1)^2} \quad (32)$$

$$v = \frac{\overline{Q_s}}{\overline{Q_o}}$$

$$z = \frac{CV_s}{CV_o} = \frac{\frac{\sigma_s}{\overline{Q_s}}}{\frac{\sigma_o}{\overline{Q_o}}}$$

Where  $r$  is the maximum (potential) value for the KGE if the other components achieve their maximum value,  $v$  is the ratio between the mean simulated,  $\overline{Q_s}$ , and mean observed runoff  $\overline{Q_o}$  i.e. the bias,  $z$  is the coefficient of variation of the simulated  $CV_s$  divided by  $CV_o$ . The coefficients of

variation ( $CV_s$  and  $CV_o$ ) is found by divided the standard deviation of the simulation,  $\sigma_s$ , or observation,  $\sigma_o$ , by its mean value  $\overline{Q_s}$  or  $\overline{Q_o}$ .

Ritter and Muñoz-Carpena (2013) suggested a standard criterion for the range of values that indicate when model performance is *acceptable*, *good* or *very good*, where an NSE of 0.65-0.80 is *acceptable*, 0.80-0.90 is *good* and above 0.90 is *very good*. Based on reviews of several studies of hydrology and model evaluation methods, Moriasi et al. (2007) recommended a lower value of acceptable NSE of 0.5, satisfactory results range between 0.50 – 0.65, good between 0.65-0.75 and very good between 0.75 to 1.00.



# Materials

## 2.3. Study area

Skuterud is located in Ås and Ski municipality in Akershus in the Southeast of Norway (Figure 4). The catchment area is approx. 4.5 km<sup>2</sup>. 60 % of the area is arable land, 28 % is forest and the rest are either bog, urban area, roads or other. Topographic values range from highest point at 406 m.a.s.l. and lowest is 91 m.a.s.l. The east side is steeper with shorter slopes than the west side (Deelstra et al., 2005). The catchment has been a part of the JOVA program since 1993 (JOVA, 2019), and contains a large database with information about runoff, nutrient and soil loss together with farming practices, soil properties and meteorological data.

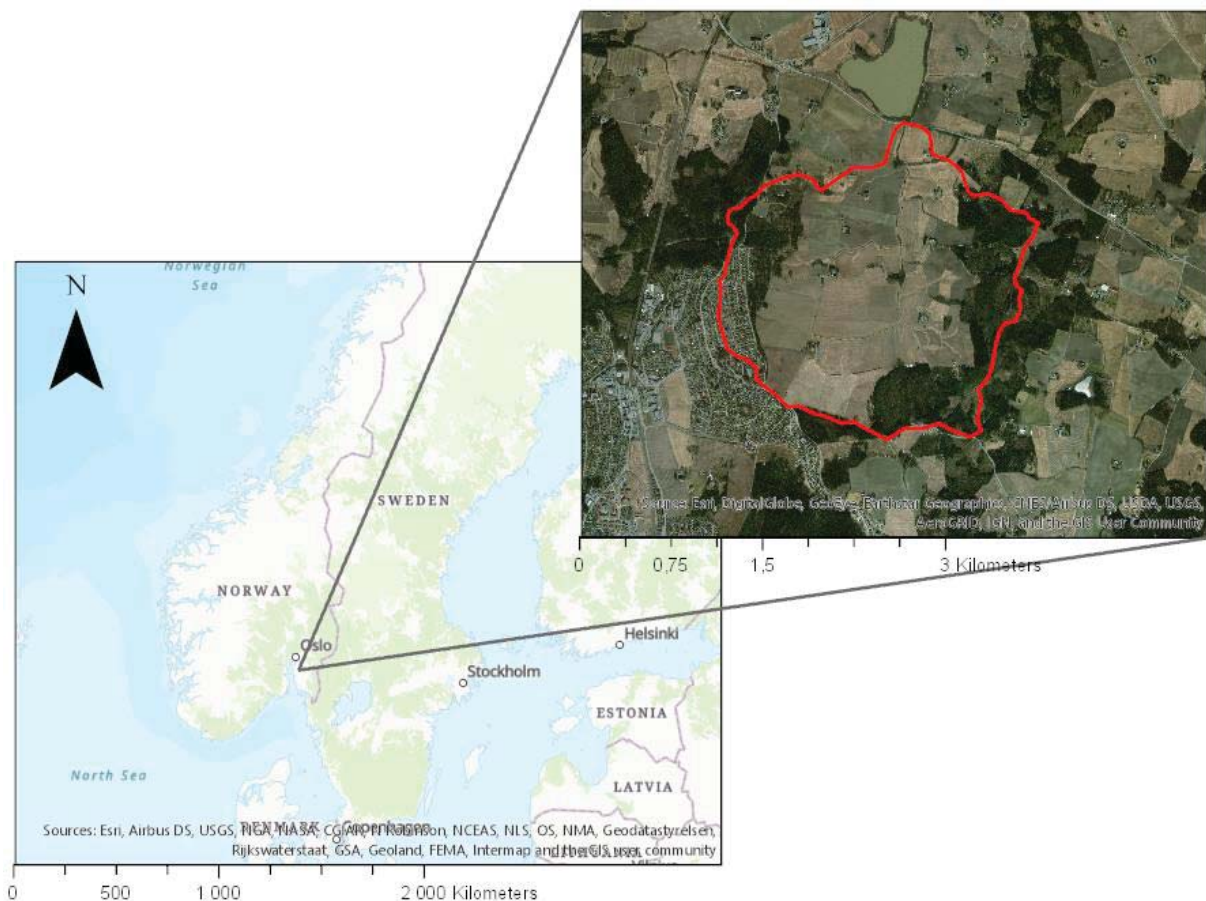
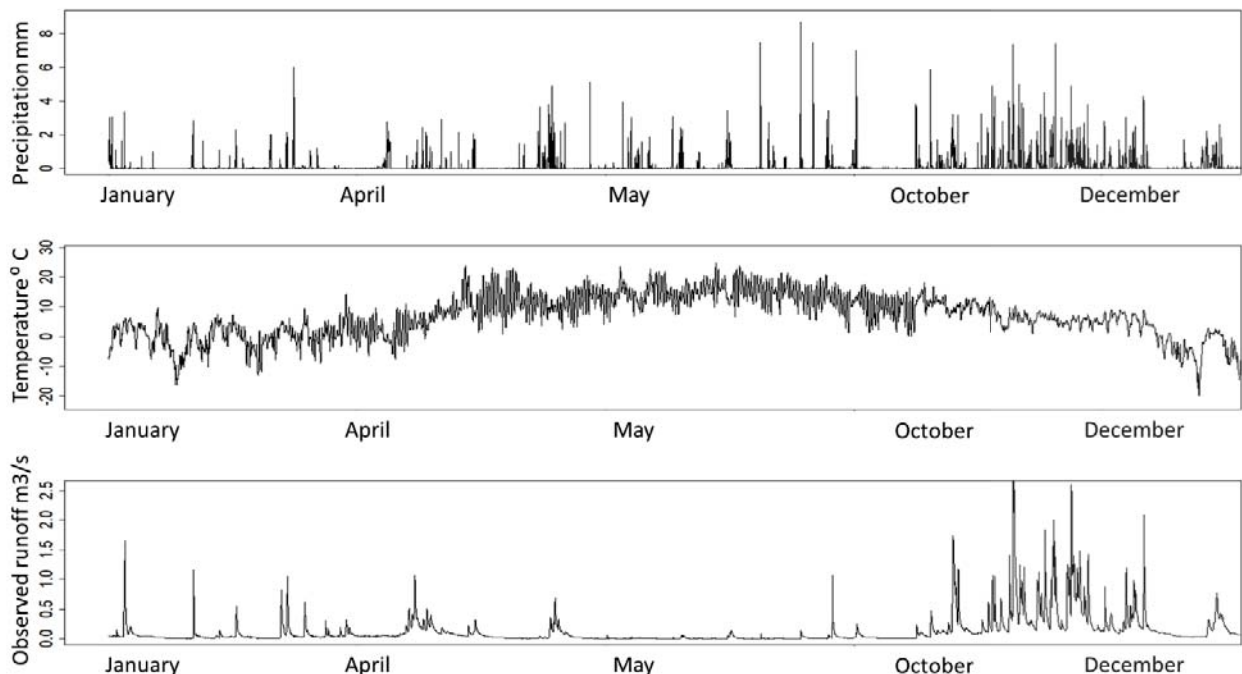


Figure 4 Location and extent of Skuterud catchment. Adapted from JOVA, 2019.

The Quaternary geology is made up of marine clay and moraine. The soil consists of mostly silty and clay loam (Deelstra et al., 2005; Fikse, 2016). The topsoil (20-30 cm) in the cultivated area is characterised mechanical mixing due to farming practices (Fikse, 2016). At 0.8 m depth, there is artificial drainage with drain spacing of approx. 8 m (Deelstra et al., 2005). The pipes are installed at different times and with different materials. The arable land is dominated by crops of wheat (80-90 %), the rest is potatoes, ley or other. 28 % of the catchment is coniferous or deciduous forest (Deelstra et al., 2005). There is a small bog located in the south of the catchment and urban area to the southwest.

The average yearly temperature between 2000 and 2009 is 6.5 °C, and average daily precipitation is 3.15 mm (JOVA, 2019). The minimum temperature during this period is usually observed between January and February and the maximum temperature is in July. The minimum precipitation is usually recorded in February and the maximum is recorded in October. The average runoff during this period is 0.08 m<sup>3</sup>/s. The highest runoff is observed in September, and the smallest is between May and August. Figure 5 shows the typical values of precipitation, temperature and runoff for one year.



*Figure 5 Observed precipitation, temperature and runoff for one year (2001) for Skuterud catchment. Data provided by JOVA (2019).*

The runoff from the catchment drains through Skuterudbekken to Østensjøvannet and Årungen and ends in Bunnefjorden (Deelstra et al., 2005). At the outlet of Skuterudbekken JOVA has a measuring station. Discharge is measured at every hour using a crump-weir.

## 2.4. Tools

### 2.4.1. R

The R project for Statistical Computing is a free software environment for statistical computing and graphics (<https://www.r-project.org>). In this study, R x64 3.5.2 was utilised to run the calibration and validation of the DDD model. R Studio, which is an integrated development environment for R, was used to create and edit code and figures (<https://www.rstudio.com/>).

Important packages for the model are the hydroPSO, hydroGOF and hydroTSM. The hydroPSO-package, where PSO stands for Particle Swarm Optimization, is developed to help users with optimization during the calibration of environmental models such as rainfall-runoff models (Zambrano-Bigiarini & Rojas, 2013). The hydroGOF (Goodness-of-fit) includes several goodness of fit functions including NSE, KGE and BIAS functions used for evaluation of environmental models (Zambrano-Bigiarini, 2017a). The hydroTSM: *Time series Management, Analysis and Interpolation for Hydrological Modelling* includes functions to analyse, interpolate and plot time series in hydrology (Zambrano-Bigiarini, 2017b).

### 2.4.2. ArcGIS

ArcGIS Pro is a professional desktop geographic information system (GIS) that allows you to view, explore and analyse spatial data (<https://pro.arcgis.com>). The program lets you work with spatial data in either raster or vector form. A raster is a spatial data model that defines space as equally sized cells, where each cell contains a value and coordinates. The vector data model represents geographic features as points, lines or polygons. Each feature is associated with an attribute and coordinates.

Important toolboxes in the distance distribution pre-process is the spatial analyst toolbox which includes a hydrology toolset to explore water flow across the surface. The toolbox includes the function *flow direction*, which finds each cells flow direction to the neighbouring cell and *flow*

*length*, to calculate the length of the flow path. The toolbox also includes the distance toolset which includes the *Euclidian distance* function used to calculate the straight-line distance from each cell to a given point or line. The conditional toolset includes the function *conditional evaluation* and provides a way to filter out data and only include distances for a specific area type. The *zonal statistics* function calculates the minimum, maximum and mean values of the distance distribution for the specific area type. Another important function is *rasterize*, which converts a vector dataset to a raster dataset.

## 2.5. Model setup

### 2.5.1. Input data

Input data in the DDD model is precipitation and temperature. Discharge measurements are used as input in the recession analysis and to evaluate the “goodness-of-fit” of the model.

Time series with precipitation and temperature originate from the measuring station at Søråsjordet (Location 1 in Figure 6). This station is owned and managed by BIOKLIM at the Norwegian University of Life Science (<https://www.nmbu.no/fakultet/realtek/laboratorier/bioklim>). It is approx. 3.9 km from the crump weir at the outlet of Skuterudbekken (Location 2 in Figure 6).

The air temperature (°C) is measured at 2 m height with a PT100 measuring station. The instrument has an uncertainty of ±0.1 °C (BIOKLIM, 2014b). Precipitation (mm) is also measured at 2 m height. The instrument, developed at NLH (now NMBU), weights the precipitation and has an uncertainty of ±0.1 mm (BIOKLIM, 2014a).

Discharge is measured using a Crump-weir at the outlet of Skuterudbekken. The relationship between the discharge and water level is explained in Deelstra (2008):

$$Q = B_c \cdot C_d \cdot C_v \cdot \frac{2}{3} \cdot \left(\frac{2}{3} \cdot g\right)^{0.5} \cdot h_1^{1.5} \quad (33)$$

Q is discharge (m<sup>3</sup>/s), B<sub>c</sub> the width of the crest (m), C<sub>d</sub> is discharge coefficient. If h<sub>1</sub> is less or equal to 0.10 m, C<sub>d</sub> is 1.163. If h<sub>1</sub> is higher than 0.10m, C<sub>d</sub> is 1.163\*(1-0.003/h<sub>1</sub>)<sup>1.3</sup>. C<sub>v</sub> is a correction factor for flow velocity at the gauging station, h<sub>1</sub> is the level measured at the control section, g is the acceleration of gravity (m/s).

Crump-weirs are commonly used in areas with high amounts of sediment transport since this usually tends to disrupt measurements when it builds up at the outlet. The crump-weir allows the sediment to be transported out. There is some restriction to the upstream section and measuring distance when installing a crump-weir. The upstream section must be straight over five times the length of the width of the crest. The water level has to be measured upstream of the crest, with a distance two times the maximum height of the water table (Deelstra, 2008).

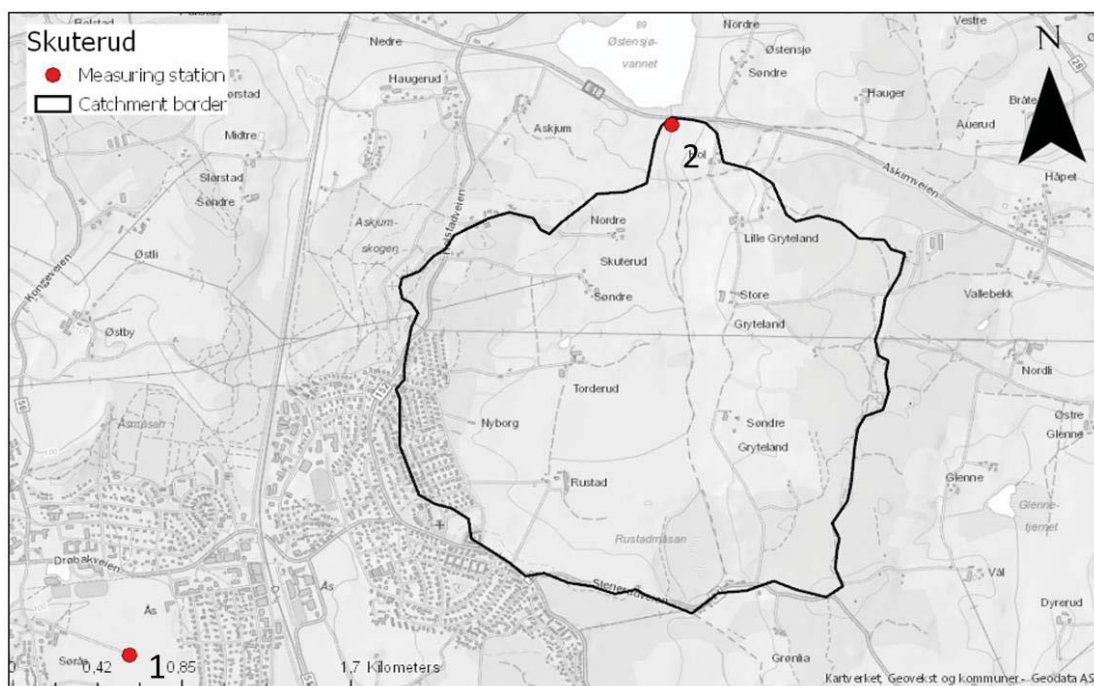


*Figure 6 Map of Skuterud catchment with location of gauging station at outlet (red dot no. 2), which is the source of discharge measurements, and the location of BIOKLIM station at Søråsjordet (red dot no. 1), the source of precipitation and temperature data.*

## 2.5.2. Model parameters

### Distance distribution parameters

The goal of the distance distribution analysis is to obtain summary statistics of the distances for points in the catchment of different area types to river network, and of points in the river network to the outlet. The distance distribution analysis describes the transport of water from hillslope to the river network and from the river network to the outlet. The results of the analysis are used as model parameters. In order to complete the pre-processing databases containing information about area types, the extent of the river and artificial drainage network, catchment boundary and digital elevation maps are needed.

Data with catchment characteristics are gathered from satellite data and downloaded in the form of vector or raster data. The river network shapefile was collected from *Elvis* at Geonorge (<https://kartkatalog.geonorge.no/>). The *Elvis* database contains information about the river network for all Norwegian catchments. All catchment elements (river, stream and water bodies) are in the form of a polyline. For the different land types, the AR50 area type database was downloaded from *Kilden*, a database managed by NIBIO (<https://kilden.nibio.no/>). The database contains spatial data of all the main land resources (forest, agriculture, urban, grasslands, bog, etc.) categorised into different classes. The DDD model categorise the catchment into *Soils*, *Bog* and *Glacier*. Only *Soils* and *Bogs* are relevant for this study. *Soils* includes all land resources except glacier and bog, and *Bog* is all land resources categorised as bog/wetland according to the AR50 area type map.

Johannes Deelstra and Alexander Engebretsen from JOVA (JOVA, 2019) provided the spatial dataset which included the location and extent of the Skuterud catchment. Follo Landbrukskontor has archives with physical drawings and maps of location and distribution of the artificial drainage system at Skuterud. In order to access these, one needs permission from the landowners at Skuterud. The plans and previous literature (Deelstra et al., 2005; Fikse, 2016) showed that the artificial drainage system is in almost every part of the arable land at Skuterud, and the distance between these are approx. 8 m, while the length of the pipes varies. To create a digitalised approximation, a grid with pixel size 50\*8m covering the arable land at Skuterud was created. A digitalised elevation map (DEM) in both 10mx10m and 1mx1m was downloaded from Kartverket (<https://www.kartverket.no/data/Hoydedata-og-terrengmodeller/>).

Two distance distribution analyses were needed in order to compare the effect of the drainage system on the model. One with a natural river network (NRN), and one with an artificial river network (ARN):

- 1) **NRN:** Distance distribution analysis with the river network as a flow path, which calculates the distances from points in the catchment to the river network, and points in the river network to the outlet.
- 2) **ARN:** Distance distribution analysis with the artificial drainage network as a flow path, which calculates the distances from points in the catchment to the nearest drainage pipe. Also, a distance distribution analysis of the points in the drainage network to the outlet.

### Recession analysis parameters

Recession analysis is a study of the decreasing part of the hydrograph and is based on runoff measurements. The aim is to find the slope,  $\Lambda$ , whenever  $Q(t)$  is greater than  $Q(t+1)$ . The distribution of  $\Lambda$  is used to estimate hillslope celerities,  $v_h$  and  $v(i)_h$ , distribution of saturation levels and storage capacity  $M$ .

A problem with the recession analysis for high temporal resolution runoff data (1h) is that there are observations of high celerities i.e. high  $\Lambda$  for low  $Q(t)$  and no clear relationship between the two. The assumption of the recession analysis is that high celerities reflect high runoff and high saturation, and that the recession characteristic is time invariant. To study this problem further several modifications for the  $\Lambda$  (*Lambda*) estimation method (LEM) are introduced:

- 1) **LEM1:**  $\Lambda$  is selected when runoff in timestep  $t+1$  is smaller than the discharge in  $t$ . This is the “original” method and is used to compare with the alternative methods: LEM2 and LEM3.
- 2) **LEM2:** To deal with the problem of high values of  $\Lambda$  for low runoff values, a screening method is suggested.  $\Lambda$  is calculated under the same assumption as before (equation 18), but the highest  $\Lambda$  values for low  $Q(t)$  are filtered out. The values that are filtered out are determined by a lower quantile boundary and is set to 0.8. The remaining  $\Lambda$ 's are used to find celerities and storage capacity.

- 3) **LEM 3:** The third solution is to create a master recession curve based on the theoretical power law relationship between  $\Lambda$  and  $Q(t)$ . The proposed  $\Lambda$  estimation method fits a line through the recession plot, and estimates the subsurface celerities and storage based on the relationship.

The parameters of the gamma distribution from LEM1, LEM2 and LEM3 are used in the calibration scenarios. The results are compared according to the individual estimated celerities, NSE and KGE results, and a test of model assumption.

### **Temporal and seasonal variation in recession parameters**

To investigate the effect of different recession lengths and seasonality of the recession analysis, an investigation of the effect of estimating  $\Lambda$  using equation 18 when  $Q(t)$  is in recess for three consecutive hours (prev. one hour) is conducted. In addition, the effect of filtering out observations with precipitation greater than 0 mm. This is done using the original LEM method (LEM1).

Also, a comparison of the difference in recession characteristics for different seasons during 2001 to examine the reason for the high variability in the recession plots. The seasons range from March 17<sup>th</sup> to May 11<sup>th</sup> (spring), May 12<sup>th</sup> to September 20<sup>th</sup> (summer), September 21<sup>st</sup> to November 19<sup>th</sup> (autumn) and November 20<sup>th</sup> to March 16<sup>th</sup> (winter).

### **Test of time invariance**

The expected value of  $\Lambda$ ,  $E(\Lambda)$ , of the gamma distribution should be time invariant and thus scale for time series of different time resolution. If  $\Lambda \sim \text{Gamma}(\alpha, \beta)$ , the expected  $E(\Lambda)$  is  $\alpha * \beta$ . The  $E(\Lambda)$  at time resolution  $m$ , should be equal to  $E(\Lambda)$  at time resolution  $n$  multiplied with value of  $m$  i.e.  $(E(\Lambda)_n/n) * m = E(\Lambda)_m$ . To check the assumption, recession analyses for aggregated time series for 3h, 6h, 12h and 24h are performed. The estimated values from each recession analysis are used to scale to lower and higher temporal resolution. The estimated and scaled values of  $E(\Lambda)$  should follow a one-to-one relationship with temporal resolution.

### 2.5.3. Model scenarios

Four model scenarios are tested and compared. The first two compare the difference between the natural river network and the artificial drainage network. Since the aim is to incorporate the artificial drainage network in the model, the altered  $\Lambda$  estimation methods are used together with the model scenario including artificial drainage network.

**NRN:LEM1:** The first calibration is done with parameters from the distance distribution of the natural river network (NRN), and celerities are estimated using the original method (LEM1). The calibration period is 2000-2004 and the validation is 2005-2009.

**ARN:LEM1:** The second calibration is with parameters from the distance distribution of the artificial drainage system (ARN). The celerities are estimated using the original method (LEM1). The calibration period is 2000-2004 and the validation period 2005-2009.

**ARN:LEM2:** The third calibration use parameters from the distance distribution of the drainage system (ARN), and celerities estimated using the screened recession estimation method (LEM2). The calibration period is 2000-2004 and the validation period 2005-2009.

**ARN:LEM3:** The fourth calibration use parameters from the distance distribution of the drainage system (ARN). Celerities are estimated using the master recession curve (LEM3). The calibration period is 2000-2004 and the validation period 2005-2009.



# Results

The results are presented in the following order: distance distribution analysis, recession analyses, and calibration and validation of model scenarios. Results from the distance distribution analyses include summary statistics and CDFs of the distance scenarios. The highlights of the recession analyses are the recession plots, the expected  $\Lambda$ , the mean celerities and the gamma distribution of  $\Lambda$  with  $\alpha$  and  $\beta$  parameters. In addition, the main findings from the investigation of temporal and seasonal variation in recession characteristics, and time invariance. The summary statistics of the distance distribution and gamma distribution parameters of the recession analysis compose the input parameter data for the four model scenarios. These are evaluated with KGE and NSE criterion. To further evaluate differences between model scenarios, excerpts of runoff simulation, and celerity and storage estimations are compared. Lastly, a presentation of the water balance components and seasonal variability of the best performing model.

## 3.1. Distance distribution

### 3.1.1. Natural river network

The results of the distance distribution from points categorised as *Soil*, i.e. all land resources except bog and glaciers, and *Bog* to nearest natural river reach are summarised in Table 2. The graph in Figure 7 shows the cumulative distribution function (CDF) of the distances from soil to the river network. The x-axis represents the distance from *Soil* to the river network and the y-axis is the fraction of the total area of the catchment. The solid line represents the actual distances, where 67 % of the total area is closer to the river network than 350 m ( $\bar{d}$ ). Figure 8 illustrates the distance distribution of points in the river network to the outlet. 46 % of points in the river network lies within the mean distance of the river network. The CDF is characterised by an almost linear increase in distances, reflecting the simple layout of the river network with few tributaries.

*Table 2 Distance distribution parameter data: Maximum distance to river network ( $d_{max}$ ), mean distance to river network  $\bar{d}_{type}$ , standard deviation ( $SD_{type}$ ), fraction of area type ( $Frac_{type}$ ) and fraction of area type with zero distance to river network ( $Z_{type}$ ).*

Type	$d_{max,type}$ (m)	$\bar{d}_{type}$ (m)	$SD_{type}$	$Frac_{Type}$	$Z_{type}$
Soil	1117	350	-	-	0,011
Bog	251	118	-	0.019	0,00230
River	2596	1442	684	-	-

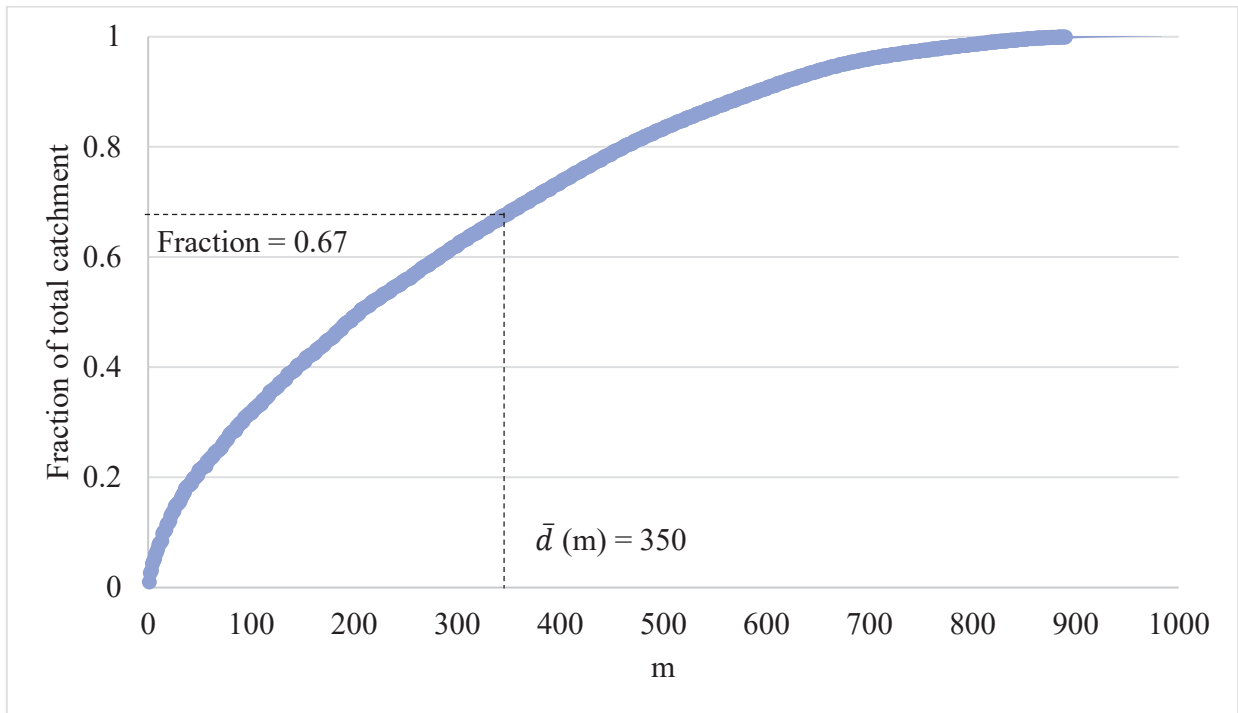


Figure 7 CDF of the distances (m) of points categorised Soil, taken from the area type map from Kilden, in Skuterud catchment to river network.  $\bar{d}$  is the mean distance.

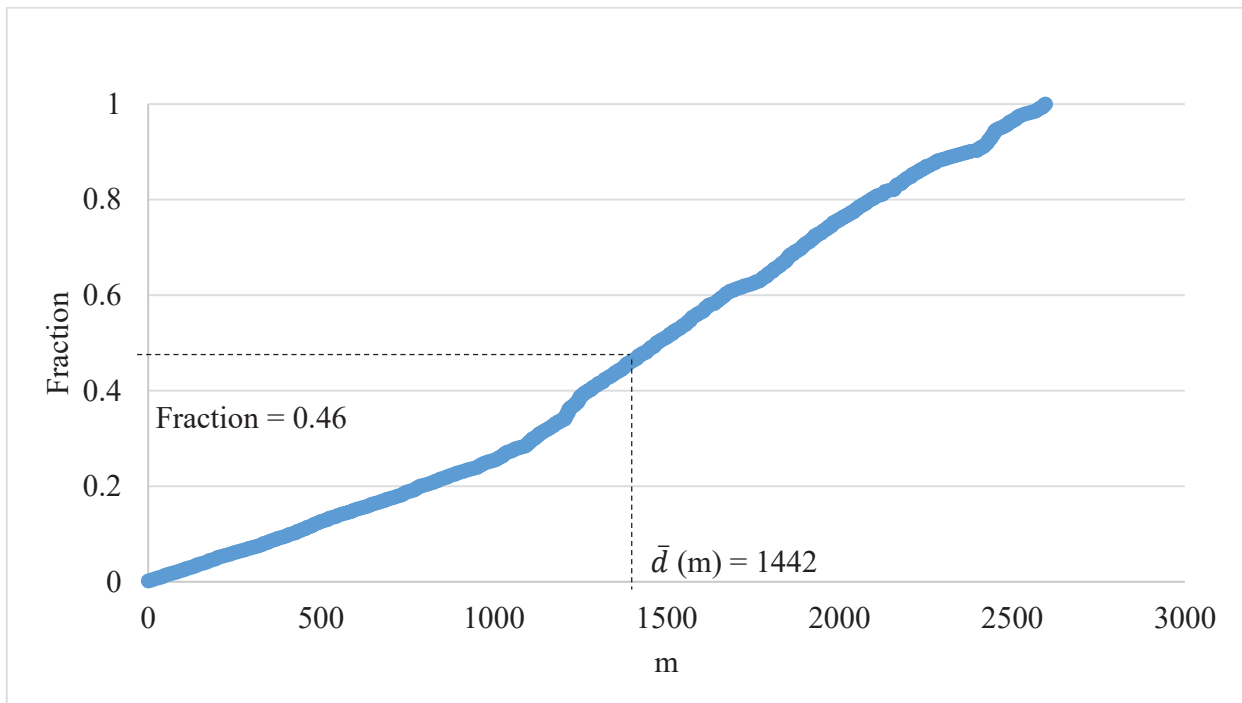


Figure 8 CDF of the distances (m) of points in river network, taken from the map in the Elvis database, to outlet in Skuterud catchment.  $\bar{d}$  is the mean distance

### 3.1.2. Artificial river network

The results of the distance distribution from points categorised as *Soil*, i.e. all land resources except bog and glaciers, and *Bog* to the nearest artificial drainage pipe are summarised in Table 3. The graph in Figure 9 shows the cumulative distribution function (CDF) of the distance distribution. The x-axis represents the distance from soil to artificial river network, and the y-axis is the fraction of the total area of the catchment. The solid line represents the actual distances, where almost 72 % of the total area is closer to the river network than the mean distance,  $\bar{d}$ . The starting point of the CDF is at 0.18, which is the value of the fraction with zero distance to the artificial river network ( $Z_{\text{soil}}$ ). 65 % of the soil is within 5 m of the artificial river network, and this is approx. the area of the arable land. The CDF of the river network is displayed in Figure 10, where 46 % of the drainage system is within 2017 m of the outlet.

*Table 3 Distance distribution parameters: Maximum distance to river network ( $d_{\text{max,type}}$ ), mean distance to river network ( $\bar{d}_{\text{type}}$ ), standard deviation ( $SD_{\text{type}}$ ), fraction of area type of total area ( $\text{Frac}_{\text{type}}$ ), fraction of area type with zero distance to river network ( $Z_{\text{type}}$ ).*

<b>Type</b>	$d_{\text{max,type}}$ (m)	$\bar{d}_{\text{type}}$ (m)	$SD_{\text{type}}$	$\text{Frac}_{\text{type}}$	$Z_{\text{type}}$
<b>Soil</b>	581	63	-	-	0.18
<b>Bog</b>	32	5.86	-	0.019	0.078
<b>River</b>	3254	2017	803.9	-	-

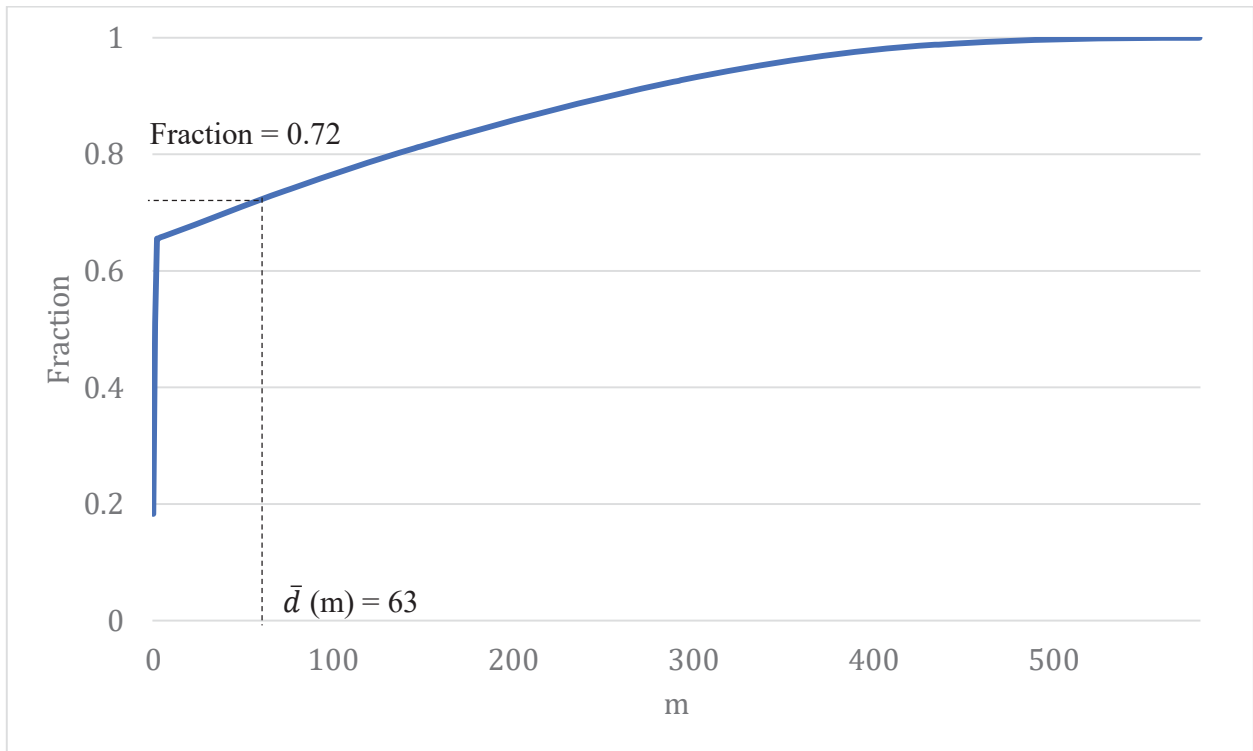


Figure 9 CDF of distances (m) of points, taken from the area type map from Kilden, to points categorised as artificial river network, in the Skuterud catchment.  $\bar{d}$  is the mean distance

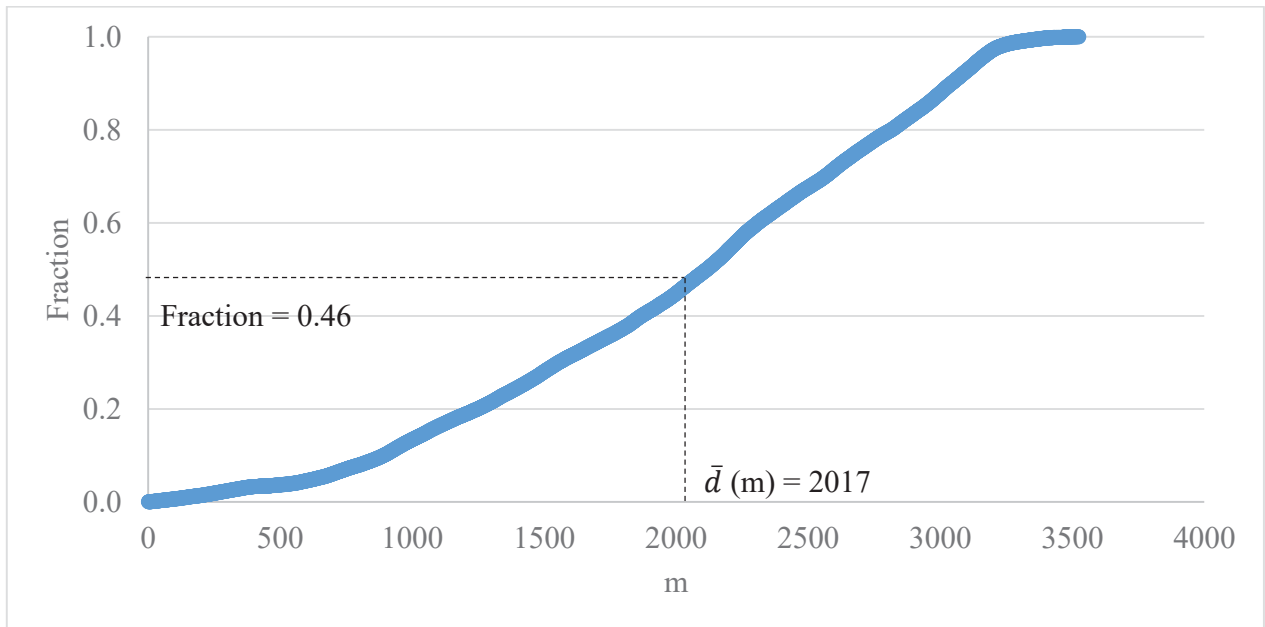


Figure 10 CDF of distances (m) of points in artificial river network, from digitalised map, to outlet, taken from Elvis database, in the Skuterud catchment.  $\bar{d}$  is the mean distance.

## 3.2. Recession analysis

### 3.2.1. Celerities

The aim of the recession analysis is to derive the celerities (m/s) and subsurface saturation levels of the catchment. The analysis is done for the calibration period of 2000-2004 with the three different methods. The mean annual discharge for the period is 0.084. Table 4 shows the summary of the recession analysis; the value of the expected  $\Lambda$  ( $\alpha*\beta$ ), the variance ( $\alpha*\beta^2$ ), and the related overall hillslope celerity for both natural (NRN) and artificial river network (ARN) estimated using equation 19. LEM2 estimates the highest  $\Lambda$  and mean celerity. LEM1 estimates the lowest  $\Lambda$  and mean celerity, while LEM3 has the lowest variance and almost equal  $\Lambda$  and mean celerity as LEM1.

*Table 4 Summary statistics of the recession analysis using the three different methods: LEM1, LEM2 and LEM3. The values are the representative mean values of the expected  $\Lambda$  and its variance, the celerity for Skuterud catchment with natural river network (NRN) and celerity with artificial river network (ARN) is estimated using equation 19.*

Time period	LEM	MAD	E( $\Lambda$ )	Var( $\Lambda$ )	NRN	ARN
					$v_h$ m/s	$v_h$ m/s
2000-2004	LEM1	0.084	0.029	$1*10^{-3}$	$2.81*10^{-3}$	$5.07*10^{-4}$
2000-2004	LEM2	0.084	0.053	$2*10^{-3}$	$5.15*10^{-3}$	$9.27*10^{-4}$
2000-2004	LEM3	0.084	0.031	$8*10^{-4}$	$2.91*10^{-3}$	$5.43*10^{-4}$

Figure 11 shows the  $\Lambda$  values (left) used to fit the gamma distribution (right) and corresponding  $\alpha$  and  $\beta$  parameters used as input in the parameter file. An overall effect of the altered LEMs is a reduction in the  $\beta$  (scale) parameter and an increase in the  $\alpha$  (shape) parameter.

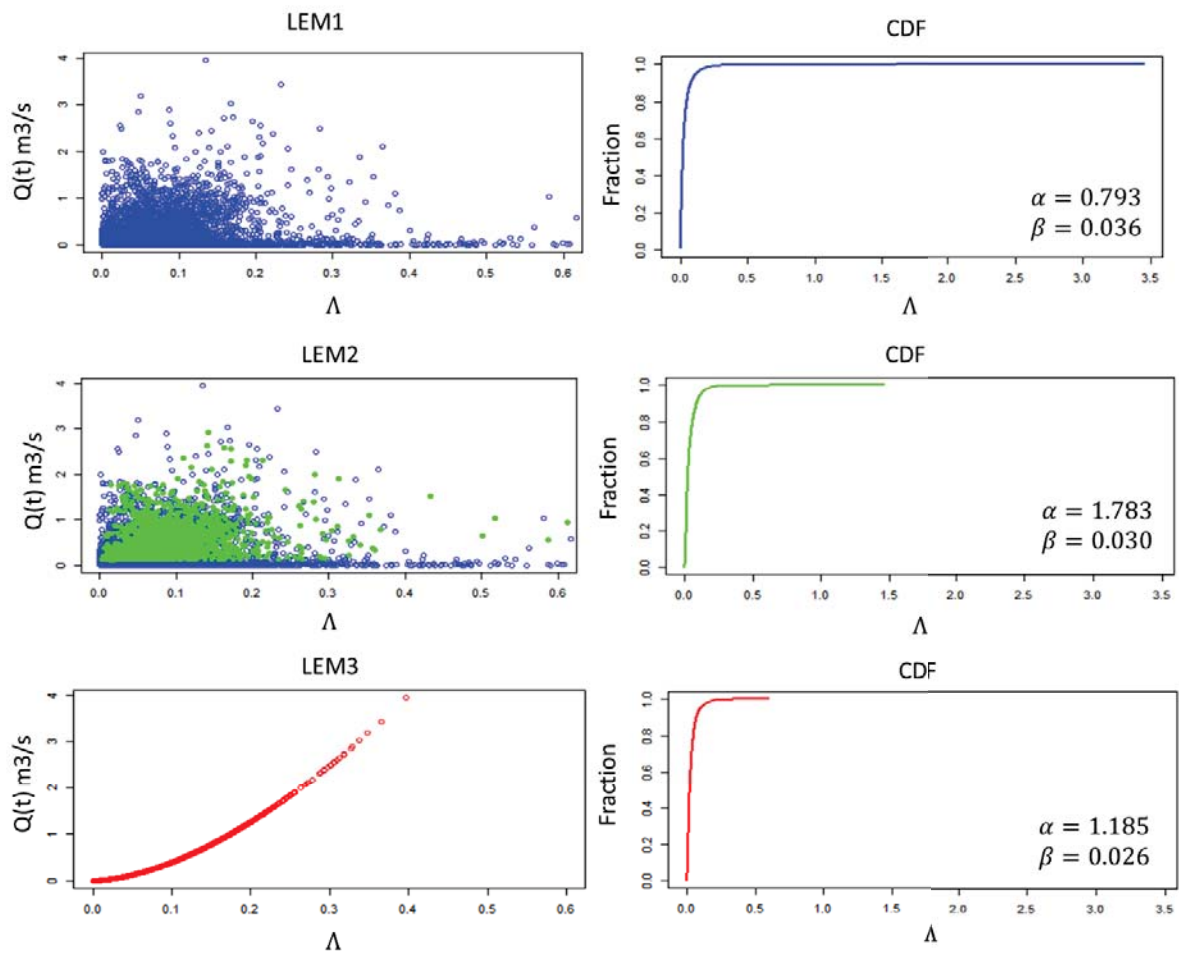


Figure 11 A selection with the corresponding CDF of gamma distribution with  $\alpha$  and  $\beta$  parameters.

### 3.2.2. Sources of temporal and seasonal variability

The method of selecting  $\Lambda$  values is important because it affects the gamma distribution and the subsequent celerity estimation. In LEM1,  $\Lambda$  is calculated whenever  $Q(t+1)$  is less than the previous  $Q(t)$ . The scatterplot (Figure 12) of  $\Lambda$  values show no clear structure with respect to the associated  $Q(t)$ , and high  $\Lambda$  values for low  $Q(t)$  for 1) recession period of one hour, 2) recession period of a minimum three consecutive hours, and 3) recession period of three consecutive hours and no precipitation. Increasing the recession period from one to three hours did not show a significant difference in the scatterplot of selected  $\Lambda$ . Filtering out runoff observation with precipitation,

reduced the max  $Q(t)$  for a given  $\Lambda$  from 4 to 2.9. It did not show a great difference in the scatterplots or estimated velocities because there were only a few  $\Lambda$  values that were filtered out.

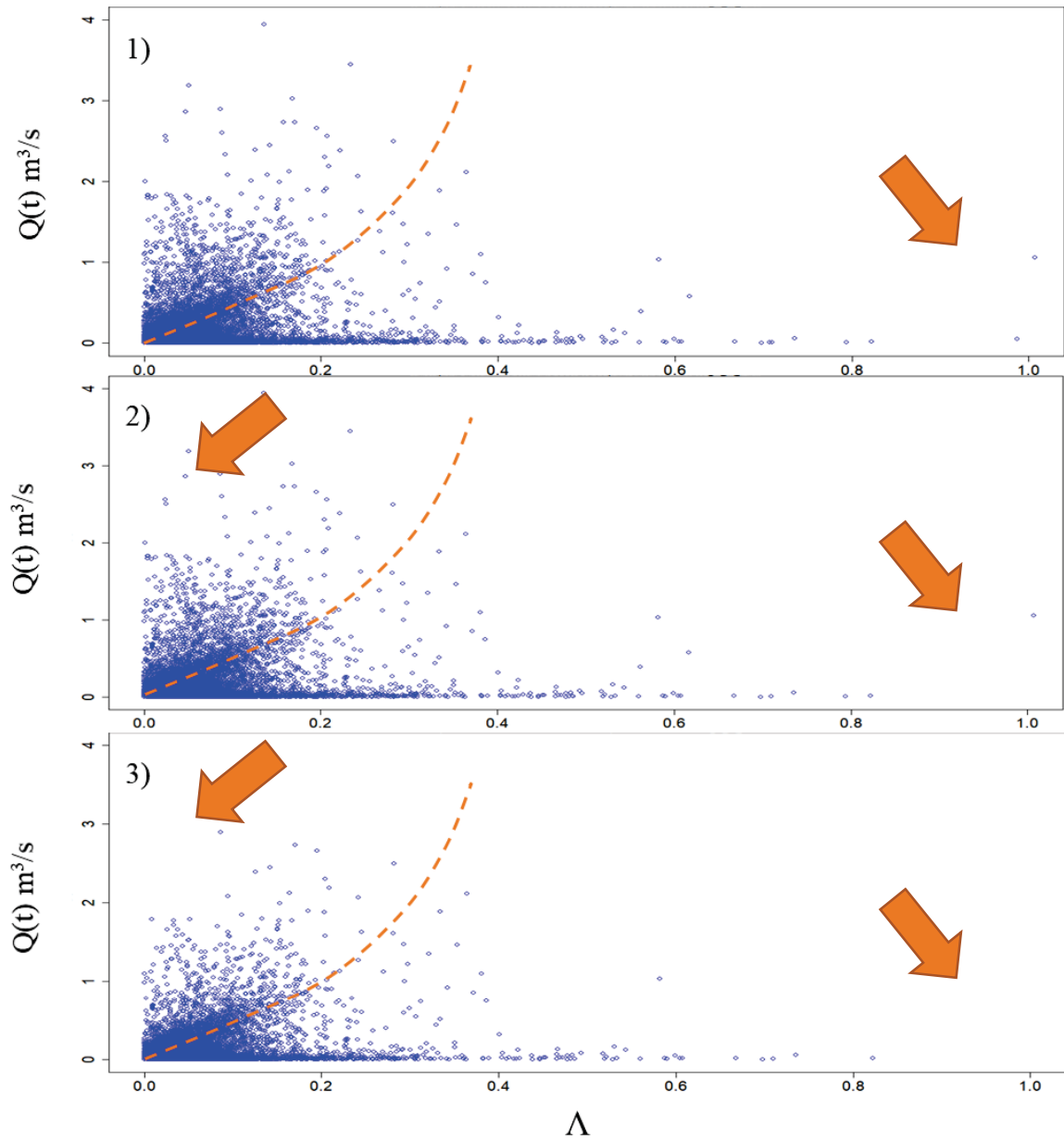


Figure 12 From top: 1) Recession segment is one hour, 2) recession segment is minimum three consecutive hours (above) and 3) three consecutive hours and precipitation is 0. The orange line is an illustration of the theoretical power law relationship that the values are expected to follow.

Table 5 summarises the recession characteristics of the different seasons. Autumn and spring have the highest mean annual discharges (MAD) and both slowest and fastest celerities. Winter and spring have the lowest MAD, but celerities are slower during winter than summer. There is no clear relationship between MAD and celerity estimation, but the lower MADs during summer and winter are reflected by lower variance.

*Table 5 Summary statistics of the recession analysis using the original method LEM1 on four different seasons during 2001/2002. The values are the representative mean values of the expected  $\Lambda$  and its variance, the celerity for Skuterud catchment with natural river network (NRN) and celerity with artificial river network (ARN) is estimated using equation 19.*

Season	LEM	MAD	E( $\Lambda$ )	Var( $\Lambda$ )	NRN	ARN
					$v_h$ m/s	$v_h$ m/s
<b>Autumn</b>	LEM1	0.14	0.019	$4.75 \cdot 10^{-4}$	$1.84 \cdot 10^{-3}$	$3.33 \cdot 10^{-4}$
<b>Spring</b>	LEM1	0.152	0.047	$3.24 \cdot 10^{-3}$	$4.56 \cdot 10^{-3}$	$8.23 \cdot 10^{-4}$
<b>Winter</b>	LEM1	0.085	0.030	$1.47 \cdot 10^{-3}$	$2.91 \cdot 10^{-3}$	$5.25 \cdot 10^{-4}$
<b>Summer</b>	LEM1	0.023	0.041	$1.76 \cdot 10^{-3}$	$3.98 \cdot 10^{-3}$	$7.18 \cdot 10^{-4}$

The scatterplots in Figure 13 to Figure 16 show the difference in  $\Lambda$  for corresponding  $Q(t)$  for the different seasons. The autumn period (Figure 13) has the least variation in observations and only a few observations when  $Q(t)$  is low. The summer season (Figure 14) is like autumn for high  $Q(t)$  but has a high count of high  $\Lambda$  when  $Q(t)$  is low. Spring (Figure 15) has the highest spread in observed  $\Lambda$ , with few structures in the observations. There is no structure in the scatterplot for the winter season either (Figure 16).

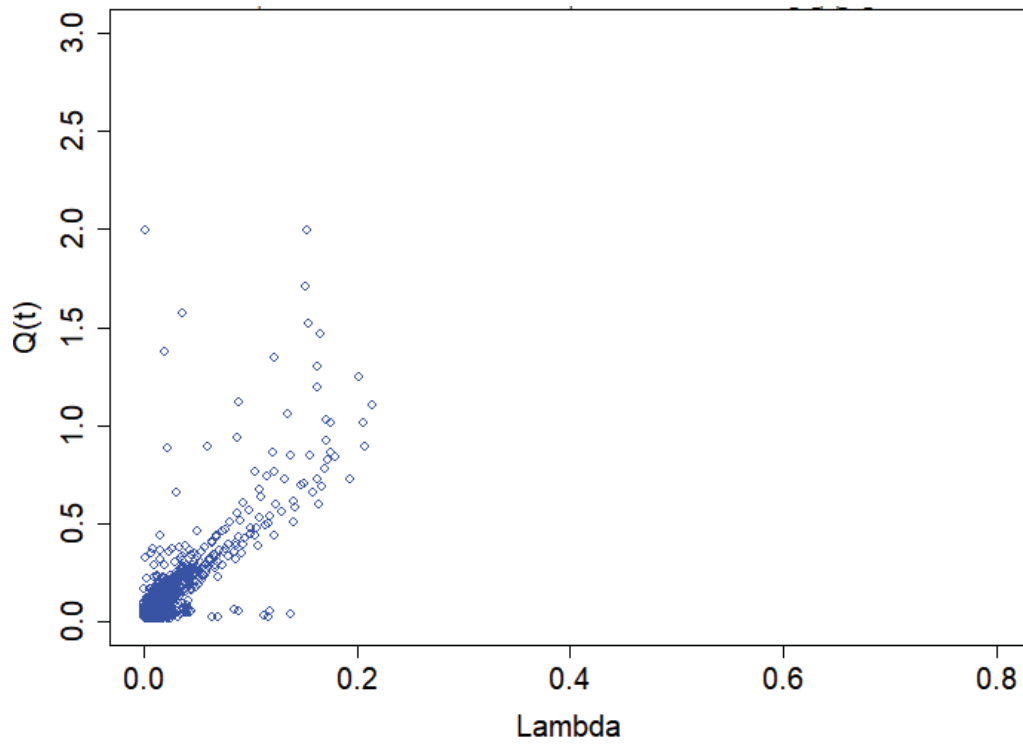


Figure 13  $\Lambda$  and corresponding  $Q(t)$  for the autumn period of 2001

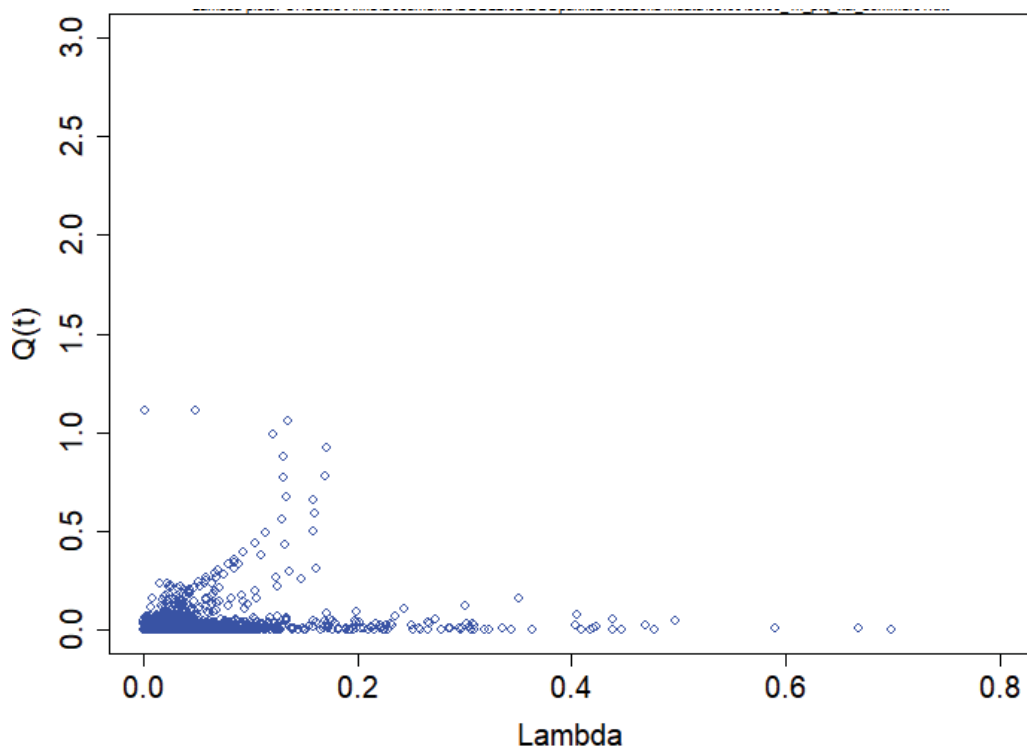
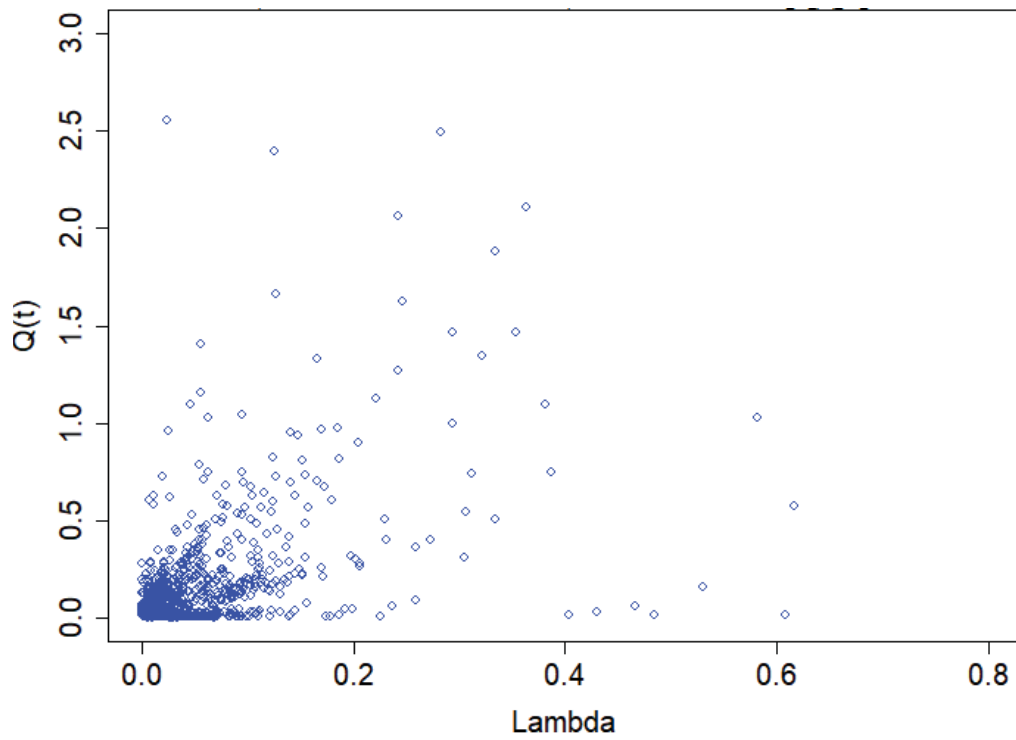
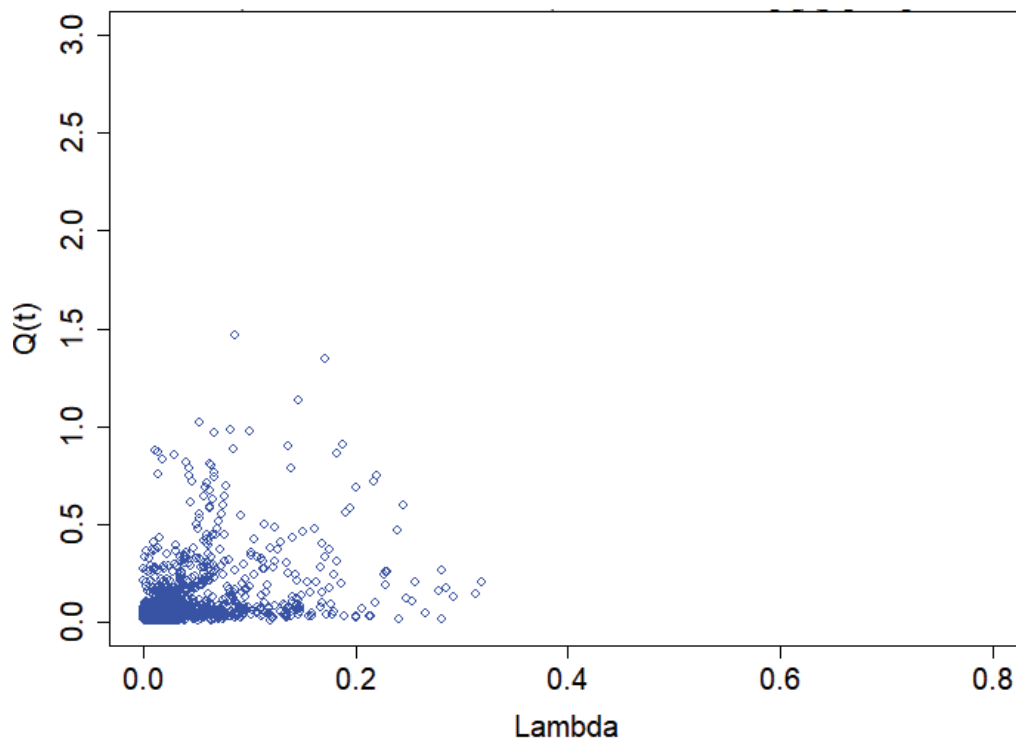


Figure 14  $\Lambda$  and corresponding  $Q(t)$  for the summer period of 2001



*Figure 15  $\Lambda$  and corresponding  $Q(t)$  for the spring period of 2001*



*Figure 16  $\Lambda$  and corresponding  $Q(t)$  for the winter period 2001/2002*

### 3.2.3. Test of time invariance

The 1h time series from 2000-2004 were aggregated to 3h, 6h, 12h, and 24h time series to test the assumption of time invariance of the recession characteristics. For all LEMs, the values scaled from 12h and 24h temporal resolution are close to the one-to-one line. LEM2 show an exponential deviation from the one-to-one line. LEM3 values are lower than those derived from the two other methods, and only values scaled from 12h and 24h fit close to the one-to-one line. The summary and results of the scaling calculation are shown in Table 6. Figure 17 illustrates the expected and scaled values under the assumption that  $E(\Lambda)$  is time invariant e.g.  $E(\Lambda)_m = (E(\Lambda)_n/n) * m$ . If estimated and scaled values are equal, they should follow the one-to-one line of the expected values.

Table 6 Expected  $\lambda$  value for aggregated time series using LEM1, LEM2 and LEM3. Values in bold are derived from analysis, other values are derived from scaling.

	$m \backslash n$	1	3	6	12	24
<b>LEM1</b>	1	<b>0.0285</b>	0.0262	0.0220	0.0114	0.0136
	3	0.0856	<b>0.0786</b>	0.0659	0.0343	0.0409
	6	0.1713	0.1571	<b>0.1318</b>	0.0686	0.0819
	12	0.3426	0.3142	0.2637	<b>0.1371</b>	0.1637
	24	0.6852	0.6285	0.5274	0.2743	<b>0.3274</b>
<b>LEM2</b>	1	<b>0.0534</b>	0.04796	0.0370	0.0253	0.0175
	3	0.16047	<b>0.1438</b>	0.1109	0.0759	0.0526
	6	0.3209	0.2877	<b>0.2217</b>	0.1518	0.1053
	12	0.6419	0.5755	0.4435	<b>0.3036</b>	0.2105
	24	1.2838	1.1510	0.8871	0.6072	<b>0.4211</b>
<b>LEM3</b>	1	<b>0.0308</b>	0.0152	0.0111	0.0065	0.0083
	3	0.0924	<b>0.0457</b>	0.0334	0.0196	0.0248
	6	0.1849	0.0913	<b>0.0668</b>	0.0392	0.0496
	12	0.3697	0.1827	0.1336	<b>0.0784</b>	0.0992
	24	0.7394	0.3653	0.2672	0.1568	<b>0.1984</b>

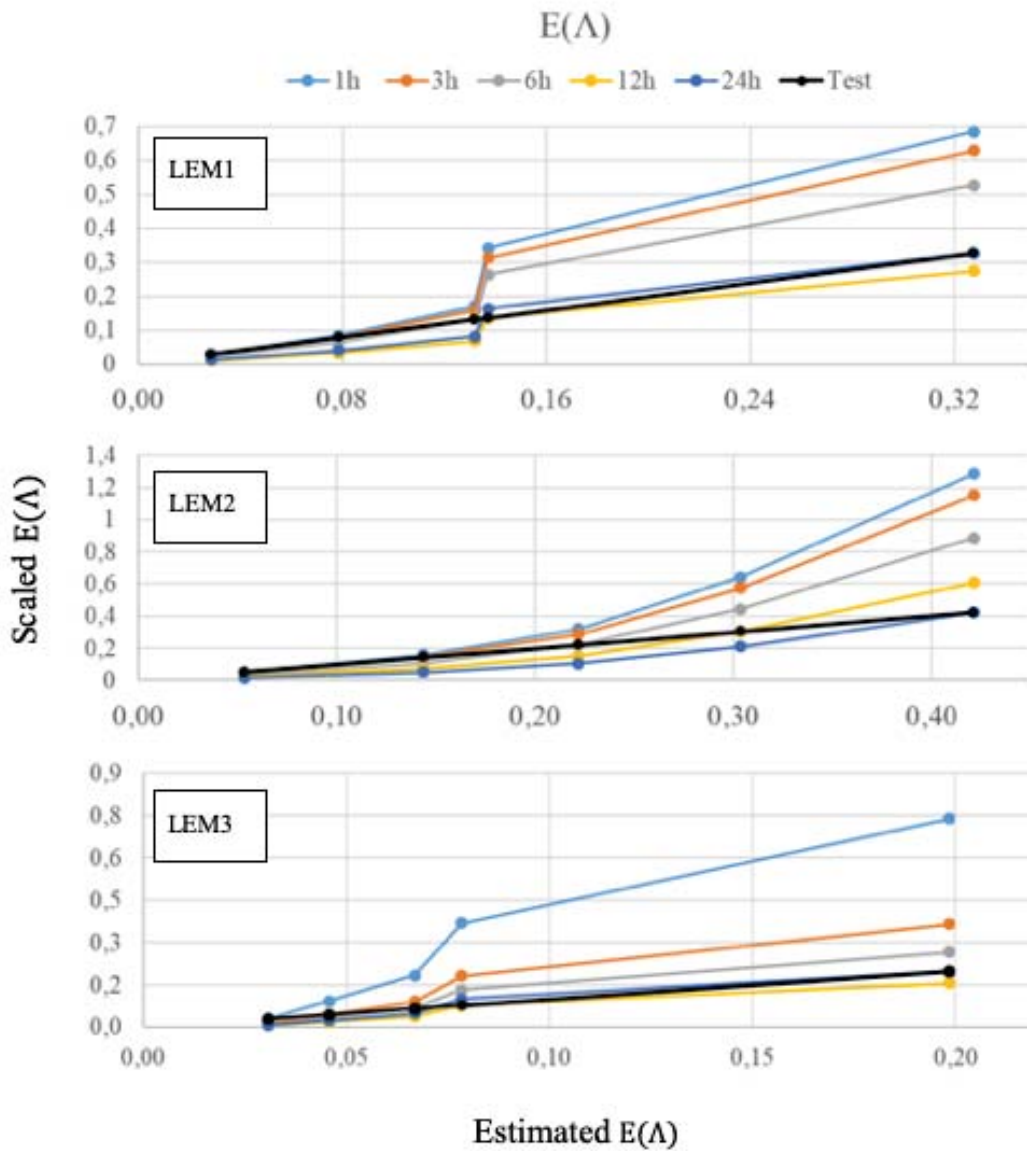


Figure 17 Plot of estimated  $E(\lambda)$  and scaled  $E(\lambda)$  values for LEM1 (top), LEM2 (middle) and LEM3 (bottom). The black line represents the theoretical one-to-one line scaled values should follow. Scaling values based on  $E(\lambda)$  of the lower temporal resolution (12h and 24h) are closer to the theoretical one-to-one line than scaled values from the higher temporal resolution (1h, 3h, 6h).

### 3.3. Calibration and validation of model scenarios

#### 3.3.1. Evaluation of the model scenarios

The parameter data from the distance distributions of NRN and ARN, and the recession analysis using LEM1, LEM2 and LEM3 were used to create the four model scenarios: NRN:LEM1, ARN:LEM1, ARN:LEM2 and ARN:LEM3. These were calibrated for the period 2000-2004 and validated for the period 2005-2009. The calibration and validation results show that scenarios using artificial river network have an overall better calibration and validation criterion. ARN:LEM1 and ARN:LEM3 has the highest NSE results of 0.56, and ARN:LEM3 has the highest KGE of 0.74. ARN:LEM3 has the overall best score and NRN:LEM1 the overall worst score. All results are summarised in Table 7.

Table 7 NSE and KGE of calibration (2000-2004) and validation (2005-2009) period.

<i>Model scenarios</i>	<i>Calibration</i>		<i>Validation</i>	
	NSE	KGE	NSE	KGE
<b>NRN:LEM1</b>	0.39	0.69	0.38	0.69
<b>ARN:LEM1</b>	0.56	0.71	0.49	0.66
<b>ARN:LEM2</b>	0.54	0.72	0.47	0.67
<b>ARN:LEM3</b>	0.56	0.74	0.52	0.72

#### Comparison of runoff simulations, and celerity and storage estimation

The simulation plots in Figure 18-Figure 21 show observed (blue line) and simulated (red line) runoff and precipitation (black line) for the different model scenarios for the time period: September 6<sup>th</sup> to October 18<sup>th</sup>, 2000. The simulations show that when adding the artificial drainage as a river network, the model estimates slightly higher flood peaks. In the selected period there are two periods of overestimation (red arrows in Figure 18). Both after periods of low amounts of precipitation. After, the models underestimate most flood peaks (green arrow). All model scenarios estimate the overall runoff dynamics and timing of flood peaks well, but tend to under- or overestimate the amount of runoff (m<sup>3</sup>/s).

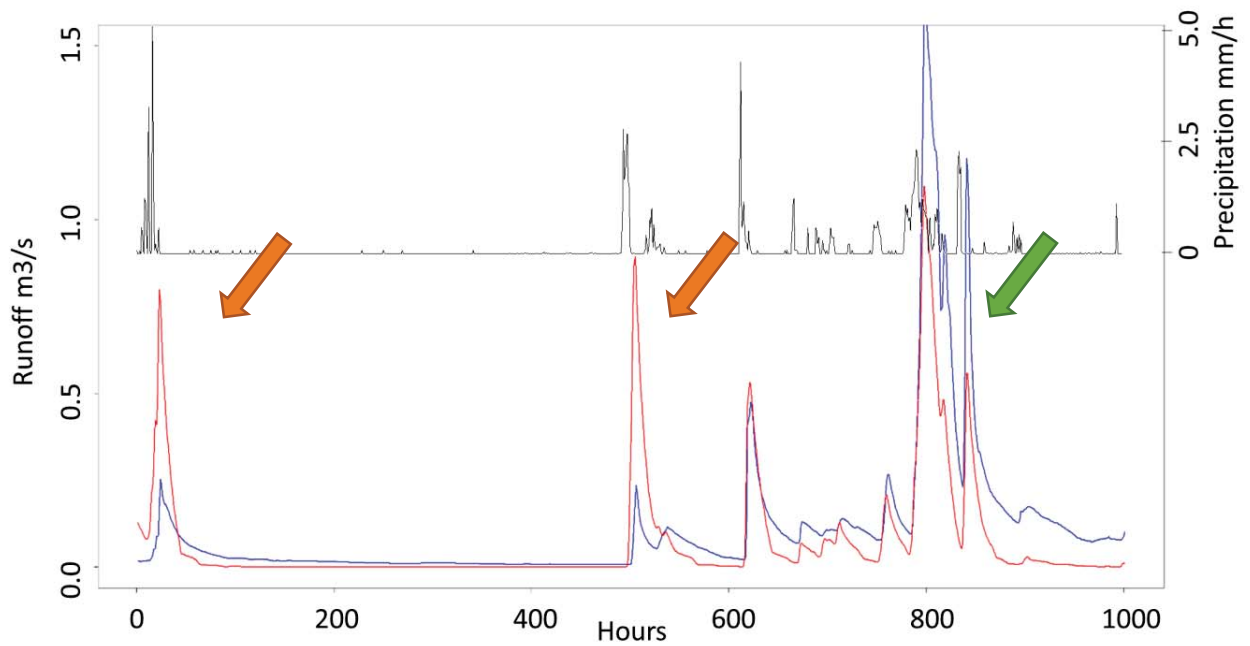


Figure 18 Observed runoff (blue), simulated runoff (red) and precipitation (black) for the time period September 6<sup>th</sup> (Hours = 0) to October 18<sup>th</sup>, 2000 using model scenario NRN:LEM1  
Arrows highlight periods of over- and underestimation of runoff. .

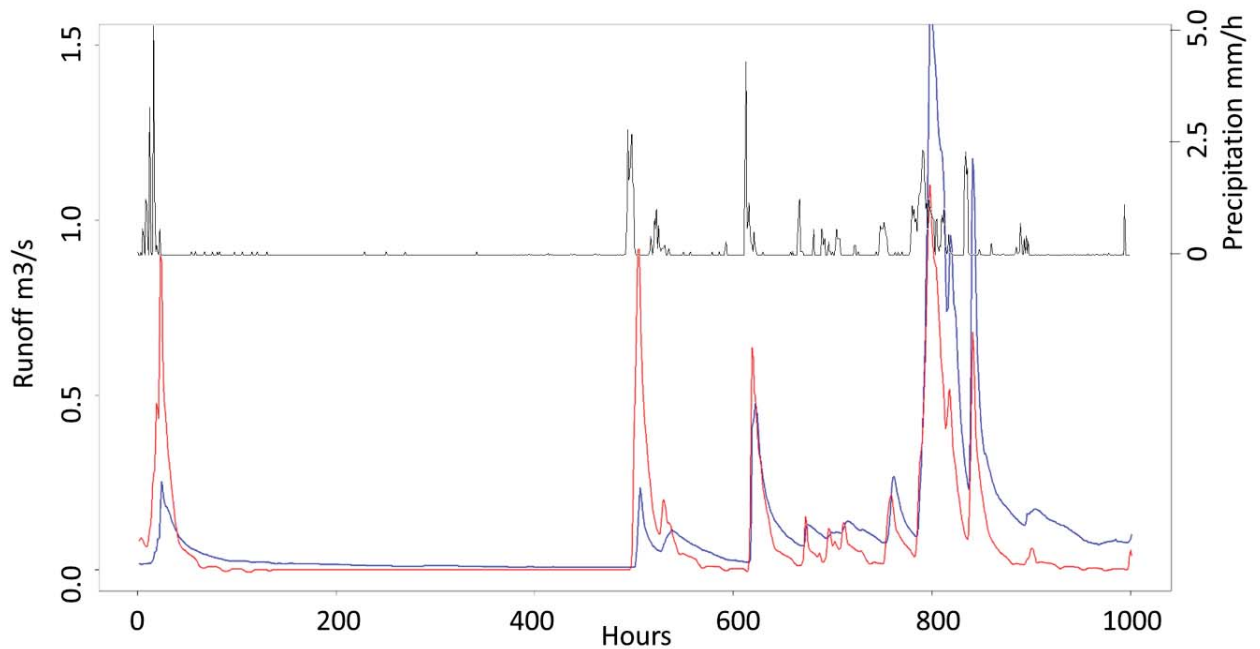


Figure 19 Observed runoff (blue), simulated runoff (red) and precipitation (black) for the time period September 6<sup>th</sup> (Hours = 0) to October 18<sup>th</sup>, 2000 using model scenario ARN:LEM1.

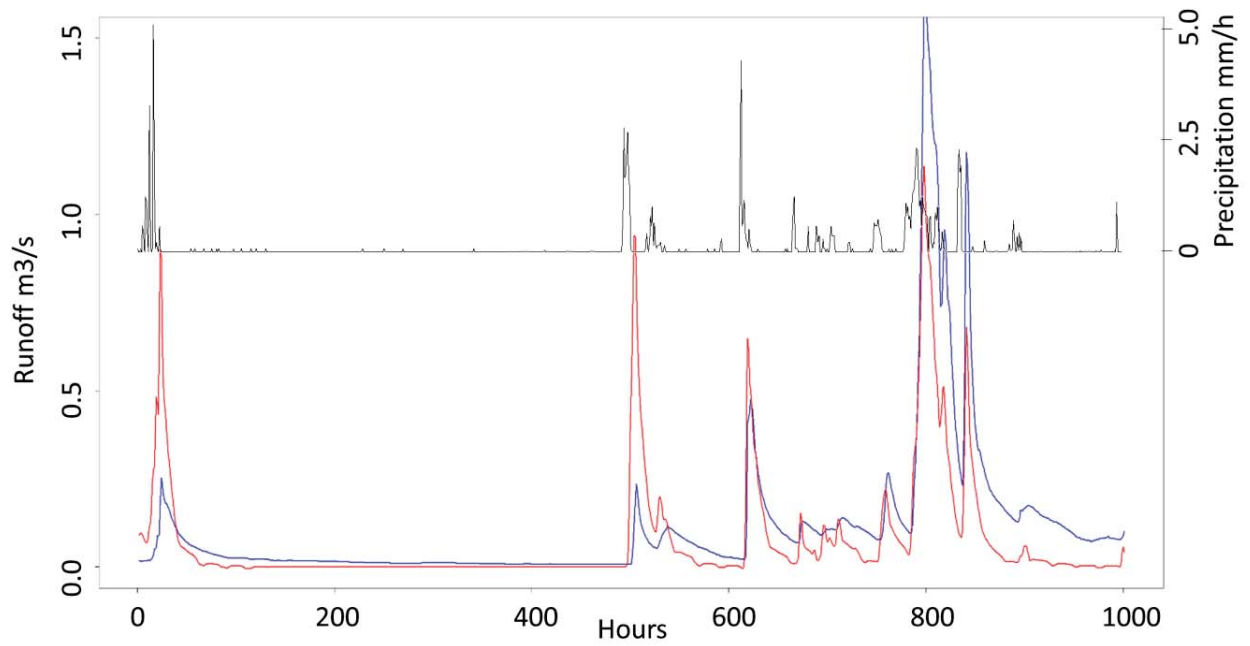


Figure 20 Observed runoff (blue), simulated runoff (red) and precipitation (black) for the time period September 6<sup>th</sup> (Hours = 0) to October 18<sup>th</sup>, 2000 using model scenario ARN:LEM2.

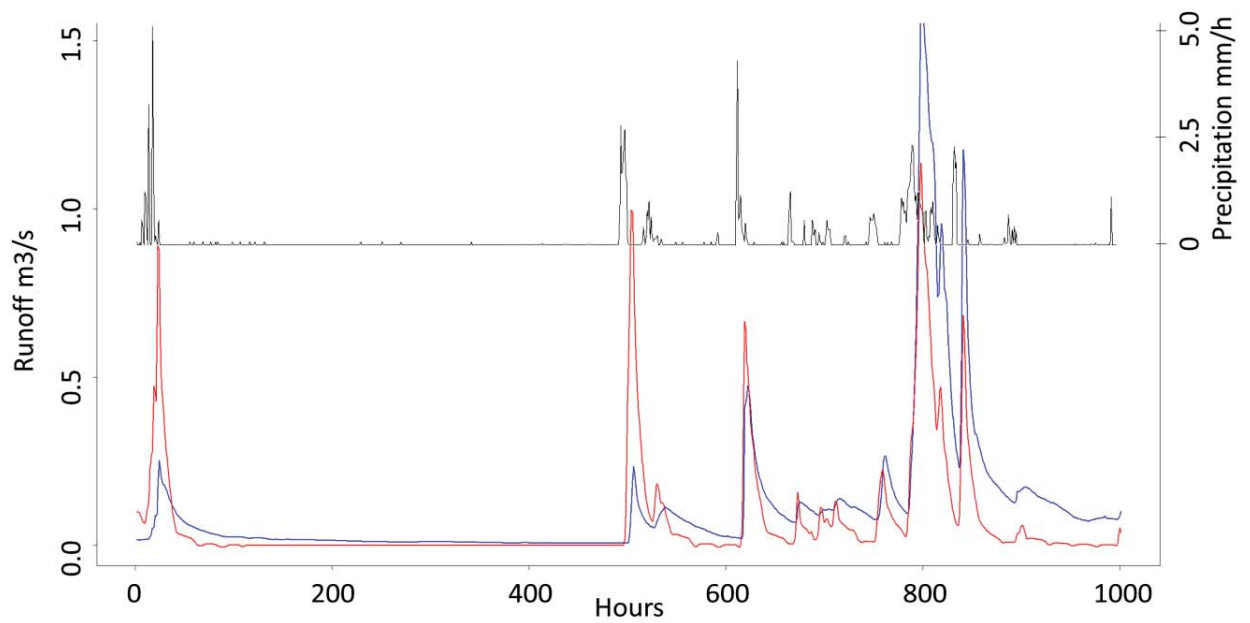


Figure 21 Observed runoff (blue), simulated runoff (red) and precipitation (black) for the time period September 6<sup>th</sup> (Hours = 0) to October 18<sup>th</sup>, 2000 using model scenario ARN:LEM3.

The estimated celerity for the saturation levels (1-5) for the different scenarios (NRN:LEM1, ARN:LEM1, ARN:LEM2 and ARN:LEM3) is illustrated in Figure 22. Level 1 is saturated conditions. All scenarios show decreasing celerities with saturation level, and celerities using the ARN-distribution is slower than NRN. ARN:LEM3 has the slowest celerity for saturated conditions, but ARN:LEM1 estimates slower celerity for decreasing saturation levels. Based on the gamma distribution and celerity estimation, each model scenario estimates a maximum storage capacity  $M$  (equation 29) of the subsurface, results shown in Figure 23. ARN:LEM1 has the highest estimate of 11.87 mm, and ARN:LEM3 has the smallest estimate of 7.50 mm.

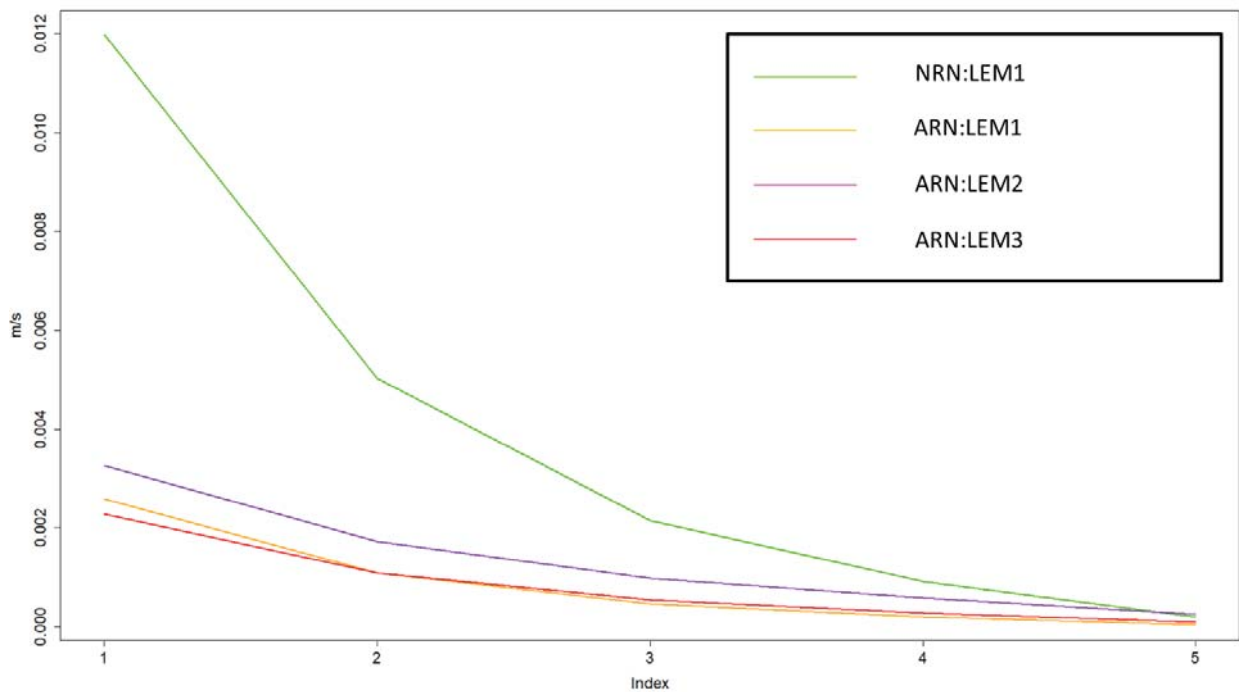


Figure 22 Estimate of celerities (m/s) for five saturation levels, where 1 is saturated conditions, for the different calibration scenarios NRN:LEM1, ARN:LEM1, ARN:LEM2 and ARN:LEM3.

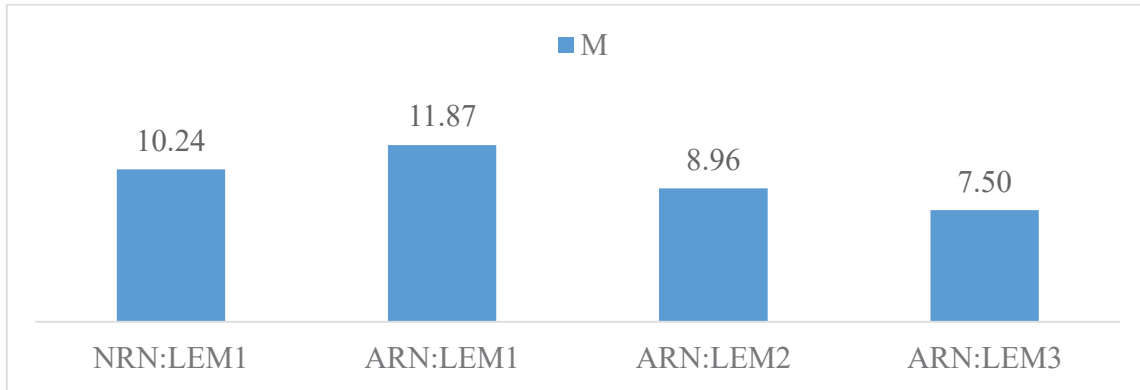


Figure 23 Estimates of subsurface storage  $M$  (mm) for the four model scenarios.

### 3.3.2. Evaluation of the best model scenario

ARN:LEM3 has the overall best score. The water balance components and seasonal variability is only presented for this model scenario.

#### Water balance components

The minimum, mean and maximum values (mm/h) of the different water balance components are shown in Table 8. The maximum change in storage corresponds to the estimated maximum capacity  $M$ . A minimum value for runoff is estimated -0.02 mm/h. Potential and actual evapotranspiration are compared in Figure 24. The actual evapotranspiration is considerably lower than the potential evapotranspiration, especially for the summer period.

Table 8 Minimum, mean and maximum values of the water balance components for ARN:LEM3

	Min (mm/h)	Mean (mm/h)	Max (mm/h)
<b><math>E_a</math></b>	0	0.01	0.37
<b>Runoff</b>	-0.02	0.06	4.31
<b>Precipitation</b>	0	0.07	24.71
<b><math>\Delta</math>Storage</b>	0	6.58	7.50

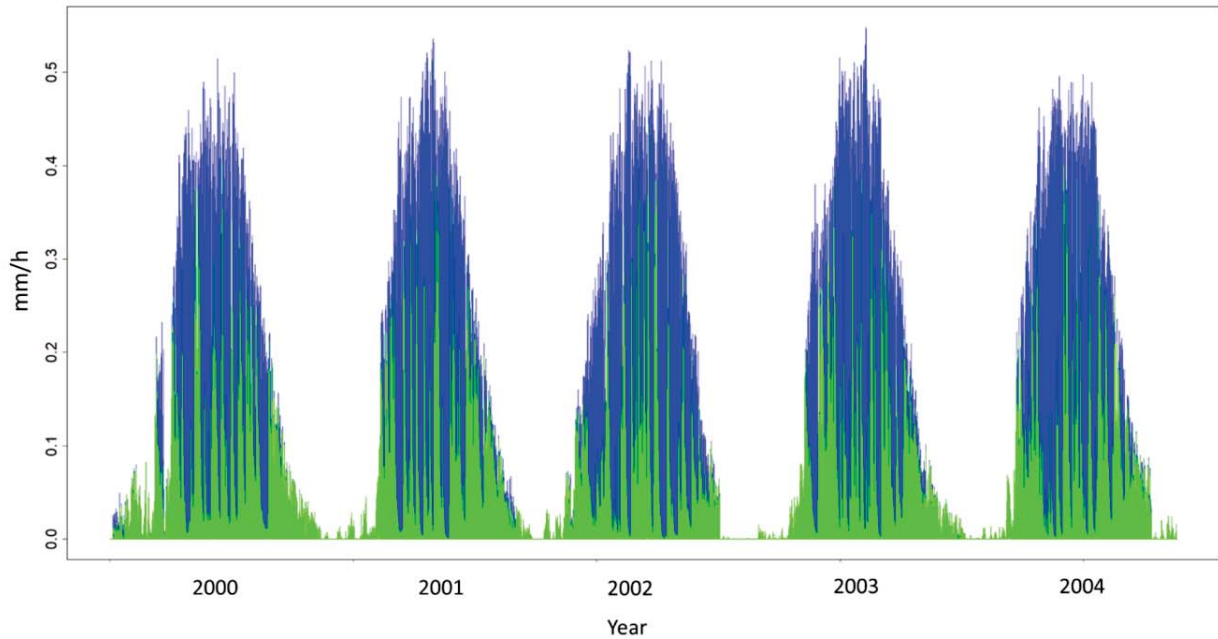


Figure 24 Potential (blue) and actual (green) evapotranspiration estimated from model scenario ARN:LEM3.

### Seasonal variability

Scatterplots comparing simulated runoff from ARN:LEM3 and the observed runoff is presented in Figure 25. The model underestimates runoff during spring and autumn, and overestimates runoff during summer and winter. The water balance for each season calculated and illustrated in Figure 26. Input is precipitation (mm),  $\Delta S$  is change in storage (mm),  $E_a$  is the actual evapotranspiration (mm) and  $Q$  is the simulated runoff (mm). Summer and spring have the highest value of evapotranspiration. The greatest contribution from storage happens during autumn and summer. The water balance is balanced for all seasons except winter, where the model estimates a total output higher than total input from precipitation and storage.

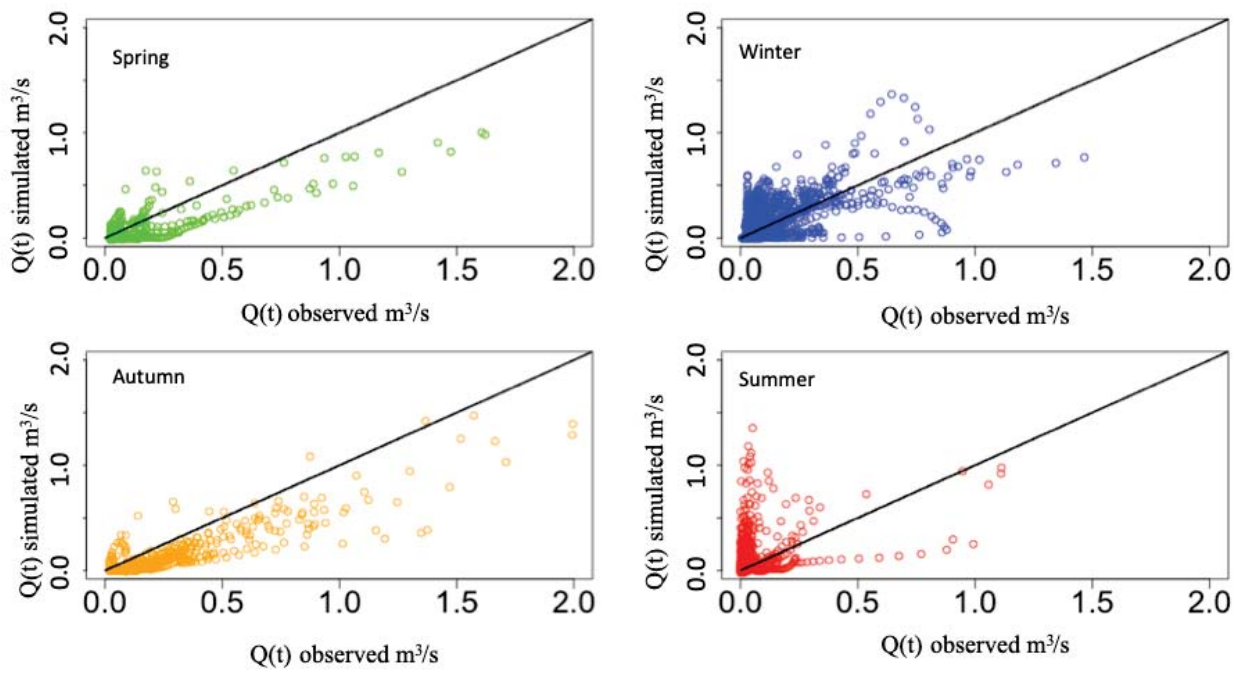


Figure 25 Observed and simulated runoff ( $m^3/s$ ) values for spring (green), winter (blue), autumn (orange) and summer (red)

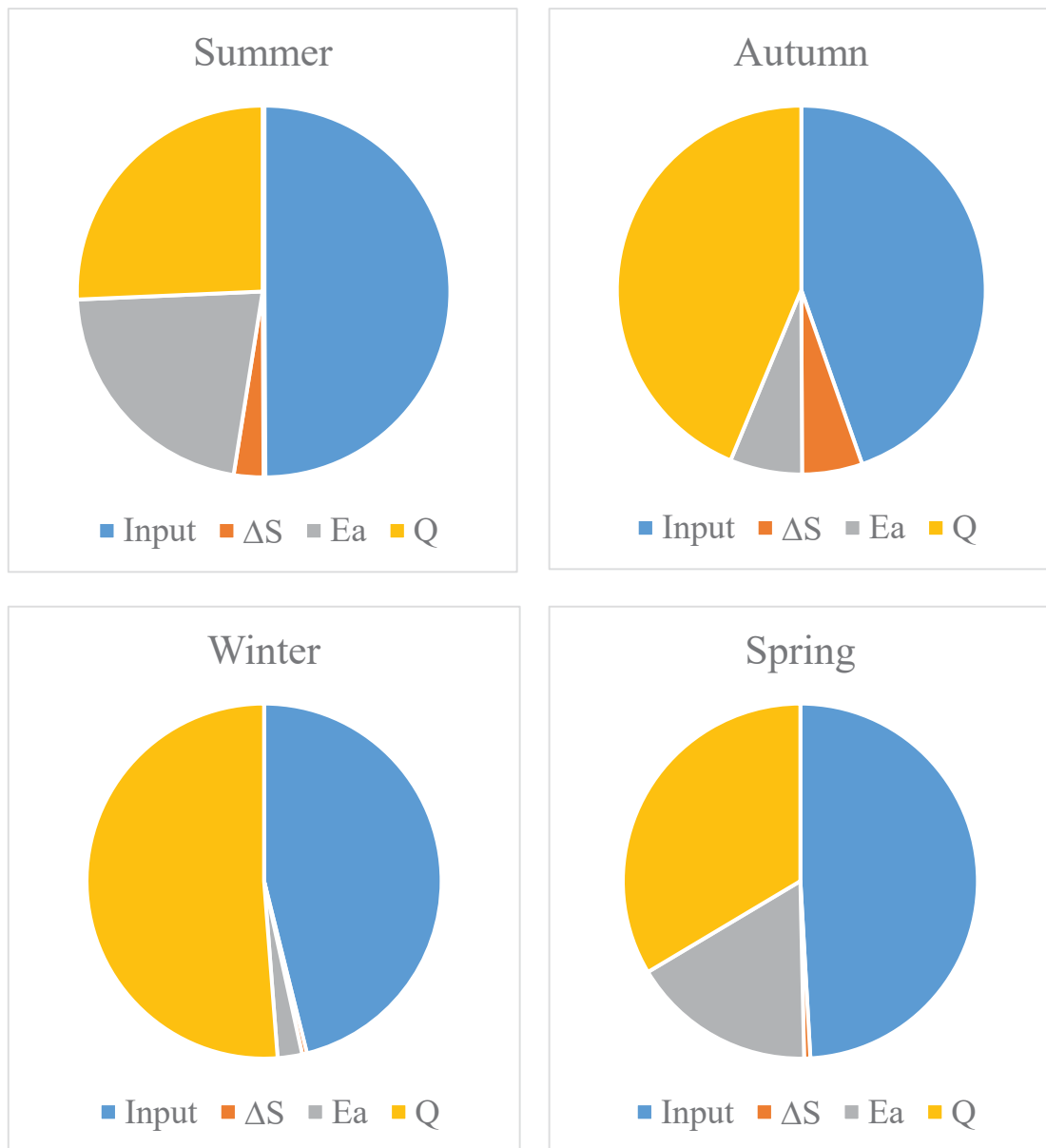


Figure 26 Water balance components (mm) for each season estimated with model scenario ARN:LEM3.

# Discussion

Modelling runoff at Skuterud on 1h temporal resolution using the DDD model proved to be a more difficult task than first anticipated. The overall best result is a NSE of 0.56 and KGE of 0.74 using scenario with artificial drainage as a river network and a master recession approach for recession analysis (ARN:LEM3). The DDD model simulates runoff dynamics and timing of peaks well, but occasionally lacks an accurate estimation of the amount of runoff.

Based on the relevant findings, the discussion section is structured around four main topics. The first two concerns findings related to the effect of changing the distance distribution and altering the  $\Lambda$  estimation method. In relation to the recession analysis, instrumental limitation at low flow combined with high temporal resolution, hydrological impact on soil characteristics and time invariance of the recession parameters are highlighted. Then, a discussion of the evaluation of the model scenarios and of the best model scenario, including water balance components, anthropogenic influences, unexpected findings and comparison to previous studies.

## 4.1. Distance distribution

The calibration and validation for Skuterud for the two different scenarios NRN:LEM1 and ARN:LEM1, revealed that the artificial drainage system as a river network improves the simulation of runoff for both calibration and validation period. The scenario with an artificial river network (ARN) improves the simulation due to a reduction of subsurface celerities. With a higher density of river network, the mean distance used in the calculation of the celerity (equation 19:  $v_h = \Lambda d / \Delta t$ ) is smaller, and the subsequent celerity estimation is slower. This improves runoff simulation and peak estimation, especially for the recession periods. In addition, the distance distribution using artificial river network increase the ratio of channel length to the total drainage area, i.e. the drainage density. A larger drainage density is characterised by quick disposal of runoff down the river network, which is reflected in more pronounced peak discharge. This is similar to the observed runoff. Using the artificial drainage system as a river network has a positive effect on the runoff modelling and simulated flood peaks.

## 4.2. Recession analysis

The major problems with the recession analysis for Skuterud are the high variability in estimated celerities for the same discharge, high  $\Lambda$  values for low discharge, and a large difference of celerities between seasons. The uncertainties could derive from instrumental limitation for runoff measurements at low flow, hydrological impact on soil characteristics and/or seasonal changes not reflected by the recession characteristics.

### 4.2.1. Instrumental limitation for runoff measurements at low flow

A comparison of  $\Lambda$ , observed runoff and precipitation are shown in Figure 27. The model assumption is that an event with a high value of  $\Lambda$  should correspond to a change between subsequent runoff observations of high value, and thus represent high saturation levels. However, in Figure 27, events with high  $\Lambda$  do not correspond with high runoff or precipitation values, but correspond to a sudden drop in the runoff to 0.0 m<sup>3</sup>/s. This happened for several events during low flow and is assumedly a result of gauging limitation at low flow, either in the actual measurements of runoff or the measurement of the water table height (Øygarden & Botterweg, 1998). There could also be physical objects such as debris, sticks, logs or ice blocking/interfering with the flow or gauging instrument (Øygarden & Botterweg, 1998). It is difficult to determine exactly what is causing the erroneous measurements since it has not been possible to monitor the gauging station during this study. Regardless, equation 18:  $\Lambda = \log Q(t) - \log Q(t+1)$  yields higher values when change between two runoff observations occur during low flow. It is when runoff is low, faulty measurements are most frequent and cause higher  $\Lambda$  values:

$$\log (3) - \log (1) = \mathbf{1.09} \quad \log (1) - \log (0.5) = \mathbf{0.69} \quad \log (0.5) - \log (0.1) = \mathbf{1.60}$$

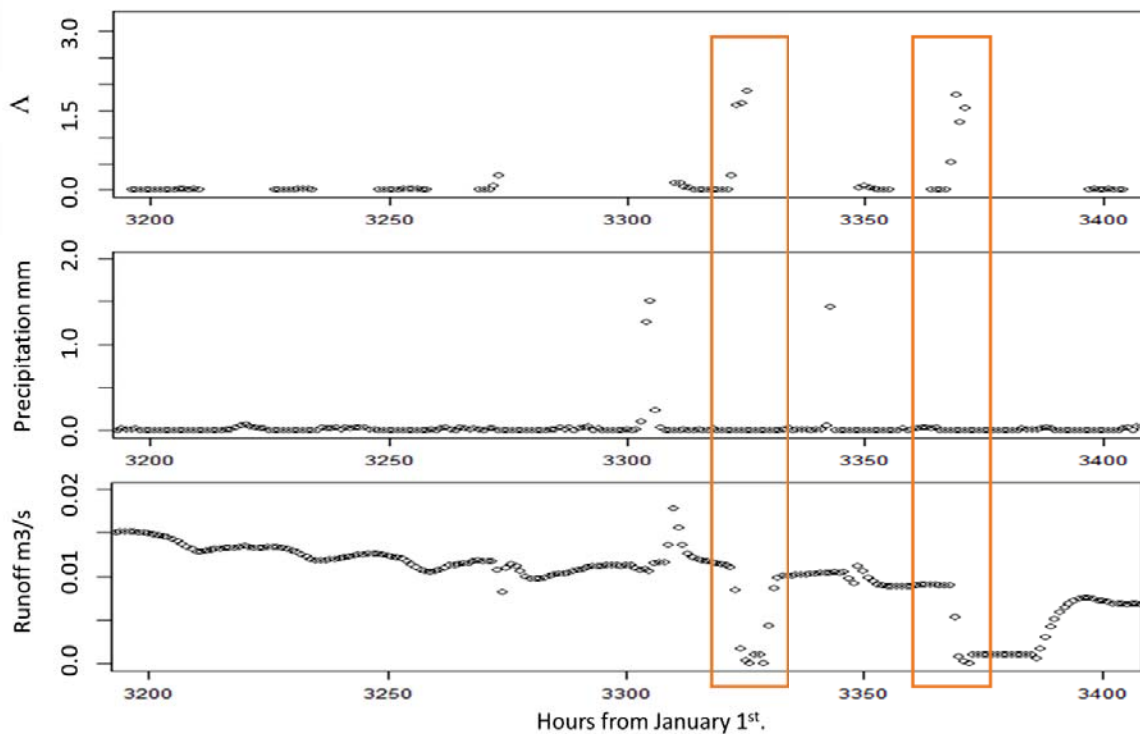


Figure 27 Excerpt of  $\Lambda$ , observed precipitation and observed runoff highlighting (inside orange boxes) where gauging measurements approach 0 and cause high values of  $\Lambda$ .

The aim of introducing LEM2 was to objectively filter out observations of high  $\Lambda$  for low runoff and fit the gamma distribution of  $\Lambda$  without these values. The results of the LEM2 recession analysis shows that there is still a lot of variation in the distribution of  $\Lambda$ . The method also estimates higher celerities than the original method LEM1. Even though the method excludes high  $\Lambda$  values when runoff is low (Figure 11), it also excludes many of the lower  $\Lambda$  values for corresponding low runoff i.e.  $\Lambda/Q(t)$  values we initially trust. This result is an overall higher celerity estimation. The lower quantile was chosen to exclude high  $\Lambda$  values close to the  $0 \text{ m}^3/\text{s}$  boundary. When the boundary is too high, the recession analysis loses all low flow characteristics, and the estimated  $\Lambda$  and celerities reflect only the higher runoff values. Overall, it seems that a lower quantile of 0.8 is too strict. One solution could be to lower the boundary to for example 0.6, illustrated in Figure 28. The estimated mean  $\Lambda$  would change from 0.056 to 0.037 and could possibly improve model results.

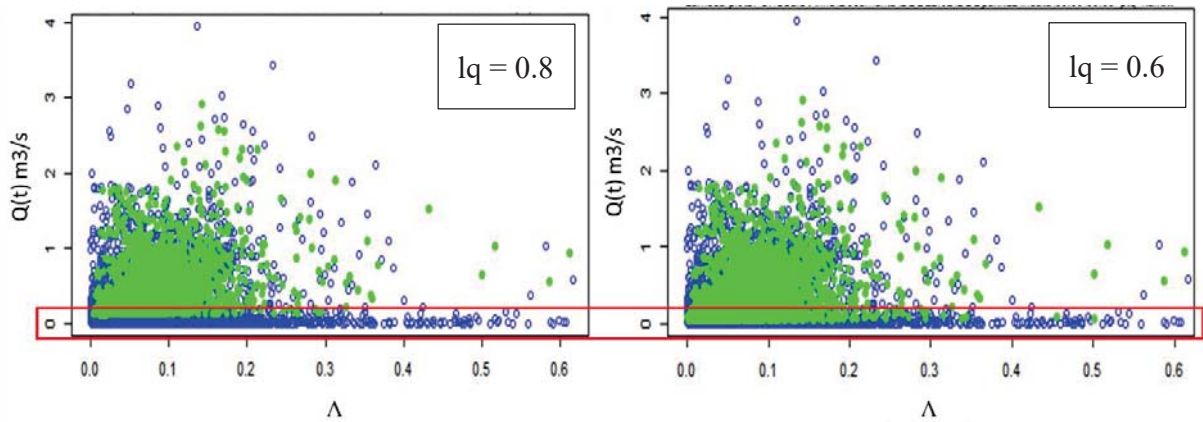


Figure 28: To the left: Screened  $\Lambda$  estimation method (LEM2) using 0.8 as the lower quantile boundary. To the right: Screened  $\Lambda$  estimation method (LEM2) with a lower quantile boundary of 0.6. Highlighted in the red box is the effect on the  $\Lambda$  selection.

Another solution to the problems related to the estimation of celerities is the LEM3. LEM3 aims to create a master recession curve following the theoretical power law relationship between  $\Lambda(t)$  and  $Q(t)$  (Figure 11). The method minimises the variance, excludes all high  $\Lambda$  values for low runoff and still manages to include recession characteristics for low runoff observations. The mean estimated celerity is not lower than LEM1 (Table 4), but the celerity for saturated conditions (Level 1 in Figure 22) is lower than all other LEMs, allowing for better simulation of recession periods and flood peak estimation. Using LEM3 in combination with artificial river network offers the best result, but the difference between the three methods is minor. Even if we filter out gauging measurements errors and fit the  $\Lambda$  values to the theoretical relationship between  $\Lambda/Q$ , the runoff simulation is still different from the observed runoff, depending on season (Figure 25) and possible wet/dry periods (Figure 21).

#### 4.2.2. Hydrological impact of soil characteristics

Recession analysis links runoff and storage dynamics. The recession parameters aim to inform about storage through the estimated celerities, based on the runoff observations. A specific recession characteristic  $\Lambda$  should be the result of the same runoff processes and storage levels. There are three possible hypotheses related to the hydrological impact of soil characteristics that

explain why this might not be the case for Skuterud: hysteresis, fluctuating infiltration capacity and seasonal inferences (evapotranspiration).

### Effect of hysteresis

One process that could explain the variability is the difference in soil characteristics during drying (desorption) and wetting (sorption) periods. The saturation level, or soil moisture content, is a function of several factors but depends greatly on the water potential of the soil. The water potential says something about the tendency of water to move from one area (vertical and horizontal) to another due to osmosis, gravity, pressure or surface tension (Slawinski, 2011). Surface tension, or capillary forces, is the ability of a liquid to flow in micropores and be retained in the soil, defying gravity. Hysteresis is the difference in water content and suction (and thus water potential) during sorption and desorption (Slawinski, 2011). The water content in the desorption part of the matrix suction – water content relationship, shown in Figure 29, is larger than water content in the wetting branch of the same water potential. This effect is due to differences in vapor tension for different water content. Thus, for a specific level of saturation, depending on if the soil is in sorption or desorption condition, the suction of the soil could be different and yield different recession rates and celerities. The effect is especially important for clay-rich soil as these have high surface tension due to high specific surface area and micropores (Nyborg, 2008).

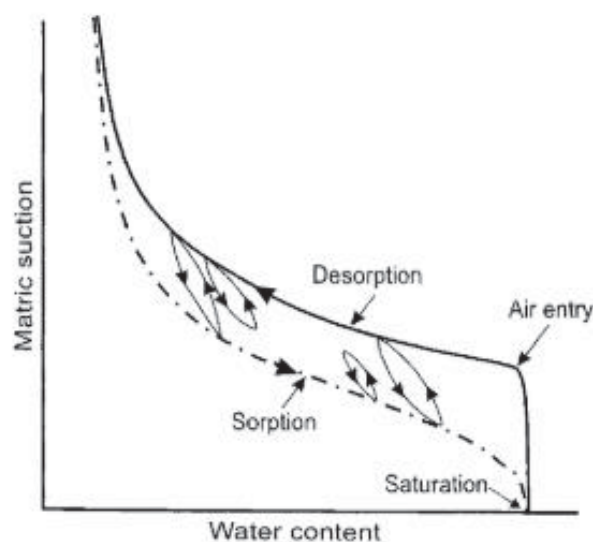
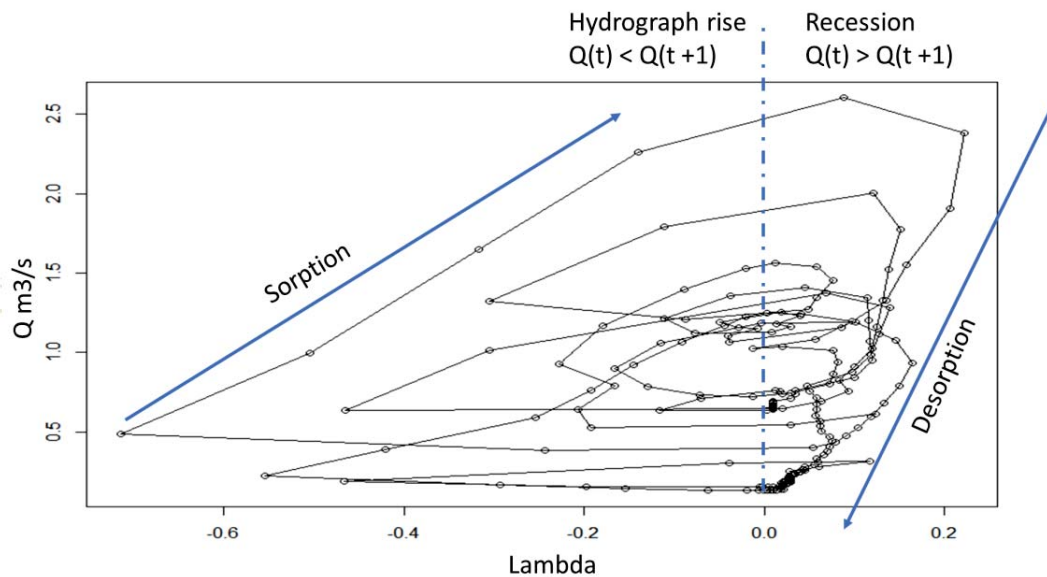


Figure 29 The suction – water content curve during desorption and sorption periods. Intermediate loops are hysteresis loops (scanning curves) (Hillel, 1998).

Figure 30 illustrates the hysteresis effect for Skuterud derived from recession analysis on the whole hydrograph. The figure shows similar trends as the water suction – water content curve, where differences in sorption, desorption and scanning curves effects the  $\Lambda$  estimation. Skuterud is dominated with soils rich in clay, and the hysteresis effect could cause runoff rates to yield different recession characteristics depending on sorption or desorption differences. The hydrograph simulations (Figure 18-Figure 21) show that the model reacts similarly after a drying and wetting period, while the observed runoff have different responses after the same periods. A reason could be hysteresis. This could also explain why there is higher variability during spring as it is likely to have more wetting and drying periods. The DDD model estimates that the distribution of  $\Lambda$  is constant in time, and even though the hysteresis effect is recorded in the recession analysis, it is not accounted for in the simulations.



*Figure 30 Hysteresis effect for Skuterud catchment derived from recession analysis when finding  $\Lambda$  for the whole hydrograph segment. To the left is hydrograph rise (sorption) and to the right the recession curve (desorption). Between the sorption and desorption lines are the scanning curves. Most scanning curves are observed when there is precipitation during the recession segment.*

## Effect of changes in infiltration capacity

Runoff generation depends on the infiltration capacity (Cerdà, 1996). The infiltration capacity is the maximum rate of infiltration to the subsurface. In runoff generation, the relationship between rainfall intensity and duration and the soils infiltration capacity plays a role in determining the amount of surface runoff, subsurface runoff, groundwater discharge and soil moisture (Cerdà, 1996). A typical pattern during a rainfall event is a decrease in infiltration capacity over time as a result of pore saturation, clogging by sediments, crust formation or swelling of the clays. Important factors determining the infiltration rates are vegetation, crust and surface cover. Cerdà (1996) found that seasonal fluctuations modified runoff volumes, runoff sources and how water is redistributed. Tallaksen (1995) observed similar trends when studying recession analysis and stated that there are in general faster recession rates in summer than autumn and winter. The differences in recession analysis for the different seasons (Figure 13 to Figure 16) could be caused by the change in infiltration capacity due to seasonal changing vegetation cover or surface conditions.

The arable catchment Skuterud has seasonally changing vegetation cover. During spring and summer, the soil is dominated by wheat and other produce, but during autumn and winter there is less vegetation. Vegetation increase the infiltration and storage capacities of the soils. They cause considerable slowing of overland flow and tend to reduce the peak flow. Cerda (1996) conducted a study of infiltration capacities of a catchment with different vegetation cover zones and through different seasons. Vegetation cover proved to play an important role in infiltration rates and could be a reason for seasonal differences in runoff and recession rates.

Another seasonal factor for infiltration capacity is temperature. The ratio of runoff to rainfall is greater during cooler months than warmer months (Figure 25) and it could be correlated to temperature differences and the effect on infiltration (Constantz & Murphy, 1991). Increased infiltration rates with increased temperature could be due to the decrease in viscosity of liquid water with increased temperature (see Figure 31). For example, Constantz and Murphy (1991) conducted a study on the temperature dependency of ponded infiltration under isothermal conditions. The study proved that there is a difference in infiltration rates at different temperatures, and the difference is greatest in the upper part of the soil.

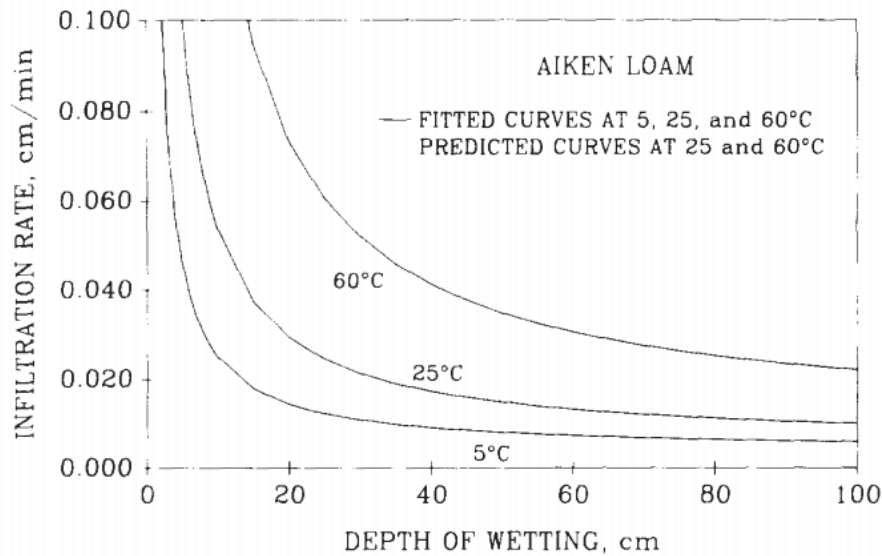


Figure 31 Infiltration rates at different temperature. Source: Constantz and Murphy (1991)

Changing infiltration rates due to changing vegetation cover and/or temperature could thus be another reason for seasonal changes in recession characteristics. The DDD model use celerities estimated from observation for the whole year. If the forces governing a certain saturation level and subsequent runoff pattern are not the same during this entire period, the derived recession characteristic and celerities are not representative.

### Effect of evapotranspiration

According to the theory of recession analysis, the characteristic of the recession segment is due to change in saturation level and drainage patterns of the subsurface alone. From the water balance calculations in Figure 26, it is evident that different sources contribute to runoff dynamics in Skuterud catchment during the different seasons. Different recession rates could be caused by different sources contributing to the stream flow, causing hydrograph rise and subsequent recession period. The value  $\Lambda$  could reflect change of another component of the water balance, for instance, evapotranspiration.

In addition to runoff, water is lost through evapotranspiration. From the seasonal water balance illustrations (Figure 26) actual evapotranspiration has a greater role during summer, and almost half of the water lost in this season is lost through evapotranspiration. During growing seasons

recession curves tend to be steep, reflecting moisture lost to streamflow by evapotranspiration, while the dormant season is characterised by flattened recession curves due to less effect of evapotranspiration (Tallaksen, 1995; Weisman, 1977). Tallaksen (1995) also identified evapotranspiration as a factor for diurnal fluctuation in recession rates with higher rates in the daytime and slower rates at night. The recession analysis for the summer period (Table 5) reflects this characterisation with higher  $\Lambda$  values than winter and autumn, reflecting steeper recession rates and higher celerities. Plotting potential evapotranspiration against  $\Lambda$  (Figure 32) for three days in august without precipitation demonstrates the diurnal fluctuations described by Tallaksen (1995), with steeper recession curves when potential evapotranspiration is higher. If there is a correlation between  $\Lambda$  and evapotranspiration it would mean that the recession characteristic does not only reflect subsurface drainage but the effect of loss through evapotranspiration.

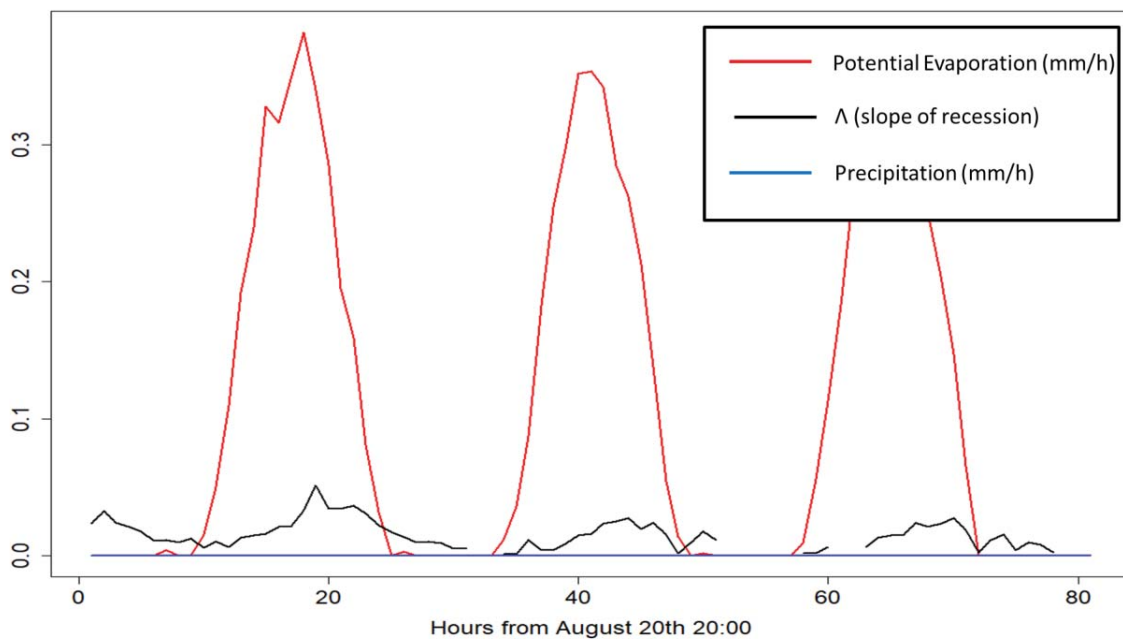


*Figure 32 Potential evapotranspiration, the slope of recession  $\Lambda$ , and precipitation for a recession period from August 20<sup>th</sup>, 2001.*

## The runoff and storage relationship

The recession characteristic is derived from runoff and attempts to inform about storage conditions. Runoff is a function of storage, and changes in storage can be estimated from changes in runoff (Kirchner, 2009). In the DDD model, the temporal distribution of storage is considered to have the same shape as the distribution of observed recession characteristic  $\Lambda$  (Skaugen & Mengistu, 2016). Figure 33 shows how the model estimates the relationship between simulated runoff and storage versus the observed runoff and estimated storage. While the simulated runoff values and storage  $M$  is approximated by a power law relationship, the observed runoff values do not correspond to the same relationship. The reason for this could be that the recession characteristics are influenced by evapotranspiration in addition to changes in saturation level. A solution could be to estimate the recession characteristics when evapotranspiration has minimal impact or to find another method of estimating celerities.

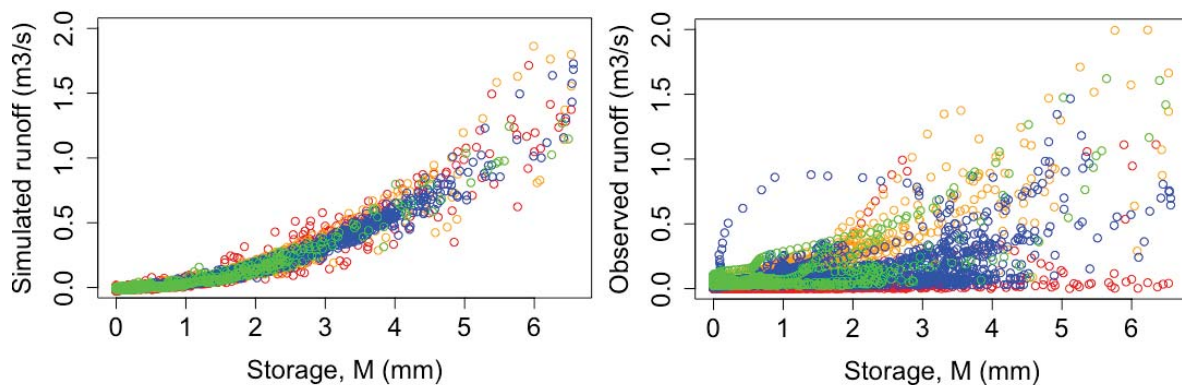


*Figure 33 Left: Relationship between simulated runoff ( $m^3/s$ ) and estimated storage  $M$  (mm). Right: Relationship between observed runoff ( $m^3/s$ ) and estimated storage,  $M$  (mm) for 2001. Green = Spring, Blue = Winter, Red = Summer, Orange = Autumn.*

Kirchner (2009) suggested two approaches which aim to minimise the effect of precipitation and evapotranspiration on recession rates. The first is to select hourly time series where runoff is 10 times larger than both potential evapotranspiration and precipitation. The second, to only use time series during night-time, since evapotranspiration rates are minimal. In this study, only the effect of selecting time series for recession analysis where precipitation was minimal was tested (Figure

12) and did not improve results. Further studies with the DDD model could test the effect of excluding evapotranspiration as well.

Another solution could be to use infiltration rates derived from fieldwork. These values reflect only the characteristic of the subsurface. Fikse (2016) did an infiltration test at Skuterud comparing infiltration at different locations. The mean infiltration rate of the study was  $5.8 * 10^{-5}$  m/s. The DDD-model estimates the lowest velocity at  $3.3 * 10^{-4}$  m/s (Table 5) during autumn. By using the mean celerity derived by Fikse (2016), it is possible to obtain the  $E(\Lambda)$ ,  $\alpha$  and  $\beta$  values.  $\Lambda$  is defined by  $\Lambda \sim \text{Gamma}(\alpha\beta)$  with the expected value  $E(\Lambda)$  is  $\alpha*\beta$ . If  $\alpha$  is equal to that of the LEM3 gamma distribution (1.185), it is possible to estimate the  $\beta$  value to 0.00279. These  $\alpha$  and  $\beta$  values can be used as input in the DDD model. Initial testing of a model scenario using these values in the parameter data suggests simulation with higher storage capacity  $M$  and slower subsurface celerities, but the method needs to be further perfected in a future study.

#### 4.2.3. Are recession values time invariant?

The assumption of recession analysis is that the  $E(\Lambda)$  is time invariant. It should be possible to scale 1h estimated values to other temporal resolutions. From the scaling plots (Figure 17) the  $E(\Lambda)$  of 1h, 3h and 6h temporal resolution overestimates  $E(\Lambda)$  when scaling to 12h and 24h temporal resolution. Scaling  $E(\Lambda)$  of 12h and 24h temporal resolution to 1h, 3h and 6h proved slightly better. One explanation could be that the higher temporal resolution includes more noise and obtains a higher estimate of the mean  $\Lambda$ , which leads to an overestimation in scaling. It would seem 1h values are not time invariant, while recession values derived from 24h values are time invariant.

Rupp and Selker (2006) studied the effect of different temporal resolutions in recession analysis. A typical recession curve has a short steep slope in the beginning and a long sleek slope at the end. They found that an appropriate temporal resolution at early recession, when change is high, might be too high when runoff recession rates approaches the limit of the gauge instrument. Likewise, a temporal resolution appropriate for late time recession might be too low for the early recession (Rupp & Selker, 2006). The noise in the recession analysis for Skuterud could be due to a temporal resolution that is too high for analysing low flow. If the main problem with the recession analysis is the gauging limitation at low runoff values, it could be solved by using 24h runoff measurements instead. These values would exclude faulty measurements during low flow.

## 4.3. Calibration and validation of model scenarios

### 4.3.1. Evaluation of model scenarios

The main difference between the four model scenarios is between scenarios using natural river network and artificial river network in the distance distribution analysis, which had a strong impact on the estimation of subsurface celerities. There was a slight difference in subsurface celerities and storage capacity estimation (Figure 23) between the model scenarios using artificial river network and different LEMs.

The NSE criterion was in the range 0.5-0.65 for ARN:LEM1, ARN:LEM2 and ARN:LEM3 for the calibration period, but only ARN:LEM3 has an  $NSE > 0.5$  for the validation period. The KGE for the same scenarios during the calibration period was  $> 0.70$ , but only ARN:LEM3 had  $KGE > 0.70$  for the validation period as well. Moriasi et al. (2007) and Ritter and Muñoz-Carpena (2013) had different views on what constitutes an acceptable efficiency criterion, but due to the model's high temporal resolution a  $NSE > 0.5$  is deemed acceptable and only the ARN:LEM3 scenario yields acceptable results for both calibration and validation period.

Compared to the result of the daily simulation of DRAINMOD, COUP, HBV, INCA and SWAT by Farkas et al. (2016) shown in Figure 34, the result from 1h temporal resolution is similar to those from the daily temporal resolution. The DDD model simulated runoff at 1h temporal resolution better than the SWAT model, and results are close to DRAINMOD, COUP, HBV and INCA. The figure shows a steadily decline in NSE with increasing temporal resolution. A hypothesis for a future study could be that the DDD model simulates runoff better on a daily temporal resolution than the previous tested models.

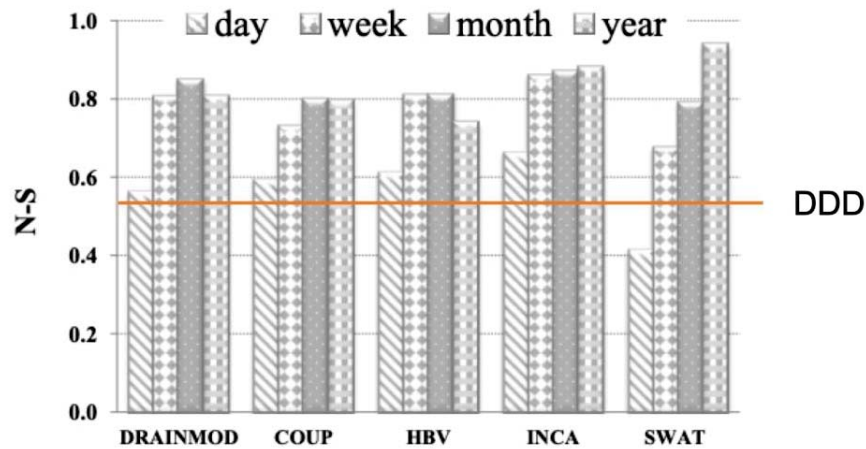


Figure 34 Results of rainfall-runoff modelling using DRAINMOD, COUP, HBV, INCA and SWAT on daily, weekly, monthly and yearly temporal resolution (Farkas, 2016).

#### 4.3.2. Differences in simulated and observed runoff values

The simulation for the ARN:LEM3 scenario (Figure 21) shows that the recession rates are higher than the observed recession, leading to a faster drop after peak discharge. The main reason why the model does not simulate recession better is due to the estimated storage capacity  $M$  (Figure 23), which is 7.5 mm. It is difficult to determine what is a realistic storage capacity, but if we assume a depth of 0.8 m (to artificial drainage), multiply this with the catchment area and a porosity of 0.2, we get a rough estimate of the subsurface capacity of 160 mm. This is considerably higher than the subsurface capacity estimated by the model. The actual storage capacity might be somewhere between these two values.

Another effect of assuming a constant maximum storage capacity is seen in the difference between observed and simulated flood peak simulation for dry and wet periods (Figure 21). The observed peak at 500-550 hours, is smaller than the simulated peak in the same interval. After several days of continuous precipitation, 800-900 hours, the observed peak is higher, while the simulated peak is almost equal in size as the peak at 500-550 hours. The precipitation at the time of the two peaks is almost the same (17 mm/h and 19 mm/h). The reason for this difference is that the estimated storage capacity is too small, and the differences between the observed runoff peaks could be due to differences in soil characteristics not reflected by the model. This is also observed in Figure 25,

where the model overestimate runoff values during summer (typically drier) and underestimate runoff during spring and autumns (typically wetter). Maximum storage capacity and water available for drainage could change during a wet and a dry period, due to sorption and desorption periods, or season (as discussed in relation to recession analysis in section 4.2.2). In the water balance equations (Figure 26) it results in a small input and output from storage.

Another consequence of the low estimation of storage capacity  $M$  is shown in the estimated amount of evapotranspiration (Figure 24). The total volume of water lost through evapotranspiration is estimated from the subsurface reservoirs  $Z(t)$  and  $S_s(t)$  and lost from  $S_s(t)$  (equation 5). When the estimate of the subsurface volume is small, the subsequent estimate of actual evapotranspiration is small. A result of this is a greater difference in the observed and simulated runoff values, especially during summer (Figure 35). The observed runoff peak could be lower than the simulated either due to higher storage capacity and/or higher amount of evapotranspiration not reflected in the model.

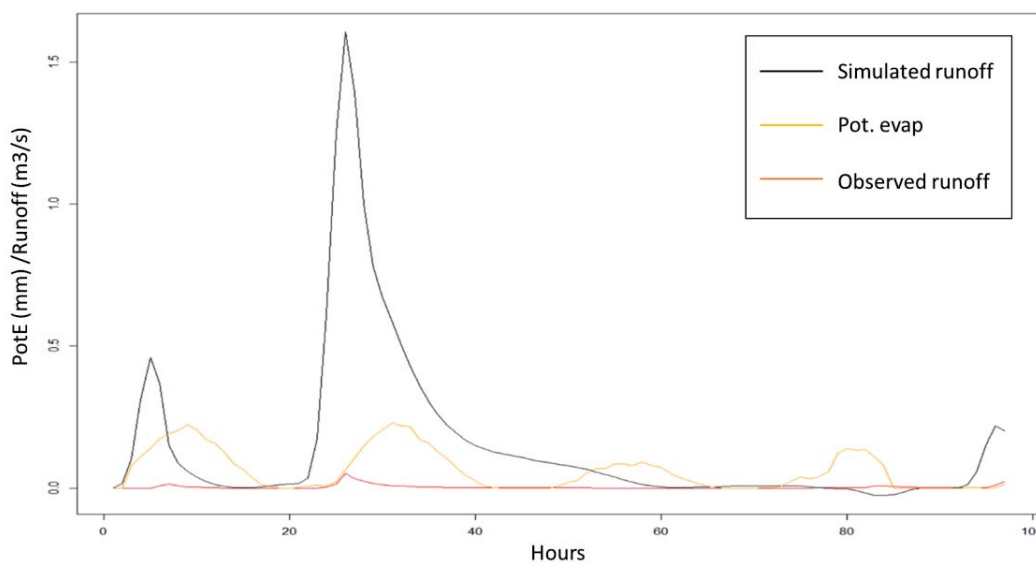


*Figure 35 Observed runoff values in red, simulated runoff values in black, potential evapotranspiration in orange.*

There could be uncertainties linked to the measured runoff and its source. The catchment is mainly arable land, and agricultural practices and anthropogenic processes could affect the runoff processes. For example, a sudden hydrograph rise could be due to a non-natural event such as

irrigation. The model only assumes input from precipitation and snowmelt, and it would be impossible to simulate runoff from an artificial input source.

Further, differences in the conductivity of the pipes could cause inaccuracies. The artificial drainage pipes were not constructed at a single point in time but is a result of work for 50+ years and is still ongoing. The pipes thus have differences in degradation and clogging. A hydrograph rise and recession could be a result of drainage through only some pipes, while the model assumes equal flow through all pipes.

Artificial drainage pipes replace natural pathways of water flow (Miller et al., 2014). The artificial drainage system intercepts the relatively slow process of interflow to the streams as most water in the upper layers of the subsurface is transported through the drainage pipes to the river network. Typical drainage in an artificially drained catchment is characterised by faster responses, reduced base flow and groundwater recharge, and higher peaks at a shorter time (Blann et al., 2009; Miller et al., 2014; Robinson et al., 1985). Deelstra and Iital (2006) noted that runoff from Skuterud has a very flashy character with large daily variations in runoff and fits the description of an artificially drained catchment well.

Modelling runoff from a catchment with responses from both natural and artificial flow pathways is complex. In this study, the problem was solved by implementing artificial drainage pipes as a part of the river network. The hypothesis was that the model would perform better, and it did, but it is still difficult to model a hydrograph rise or a sudden reduction in runoff rates that could be a result of human impact. Further, measurements of runoff could be another source of error, since it does not always reflect the natural drainage pattern and its sources, causing faulty recession characteristics and affecting the evaluation process. When incorporating the artificial drainage system in the model, it is assumed that the flow of water is equal to that of a river network. The artificial drainage network might be more complex than first anticipated, which would make this approximation erroneous.

#### 4.3.3. Unexpected findings

An unexpected finding was the simulation of negative runoff. It is illustrated in Figure 35 and Figure 36. One hypothesis is that due to the low estimate of storage capacity, when actual evapotranspiration is high, there is not enough water in the model. The observations of negative

runoff values correspond with periods of high estimates of actual evapotranspiration (Figure 36). The model estimates the actual evapotranspiration from the potential evapotranspiration and combined available water in  $D(t)$  and  $S_s(t)$  but draws the actual water from only  $S_s(t)$ . This can cause miscalculations and deficit of  $S_s(t)$ , resulting in negative values for runoff.

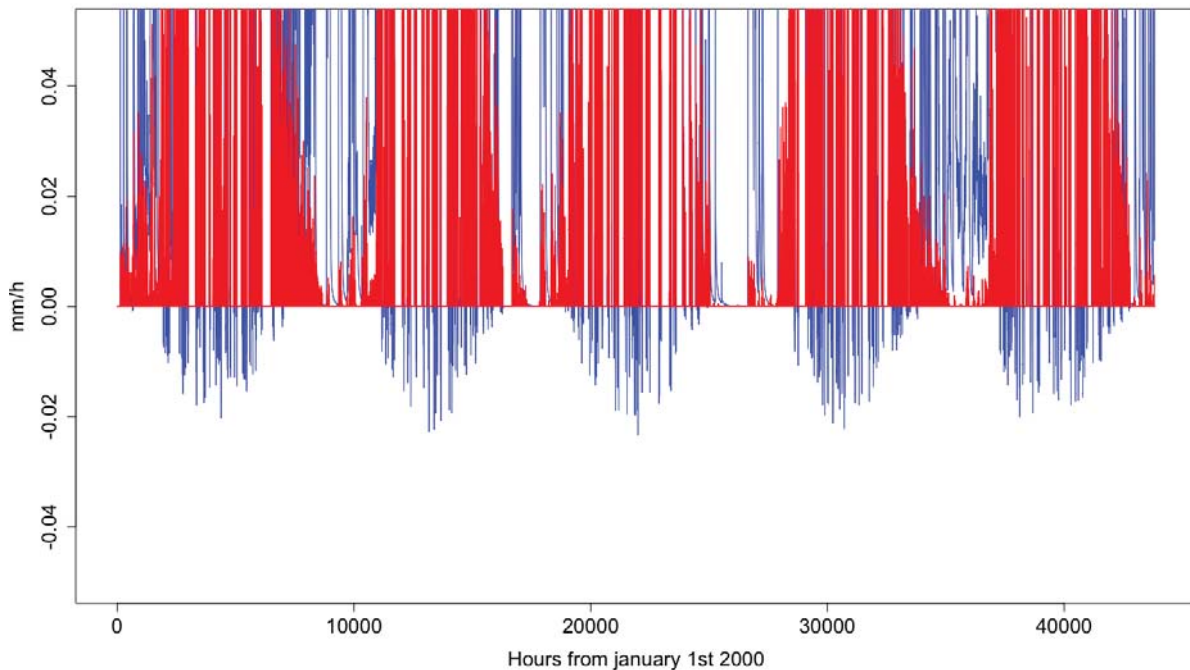


*Figure 36 Simulated runoff (blue line) and actual evapotranspiration (red line) for the calibration period 2000-2004 for Skuterud catchment.*

One of the results of the seasonal water balance for the simulation ARN:LEM3 (Figure 26) was a negative balance, with more water leaving the catchment than entering it during winter. Even though it is common for the water balance to show seasonal differences, with water deficit and water surplus, the balance between the different components is assumed to always be equal to zero. When runoff is greater than precipitation, water must come from storage, or if precipitation is greater than runoff, water is stored or lost by evapotranspiration. As seen in Figure 37, the negative water balance (black dots) corresponds to periods with high change in SWE (purple line) and could be related to an error in the snow routine or input from snowmelt in the water balance calculations.

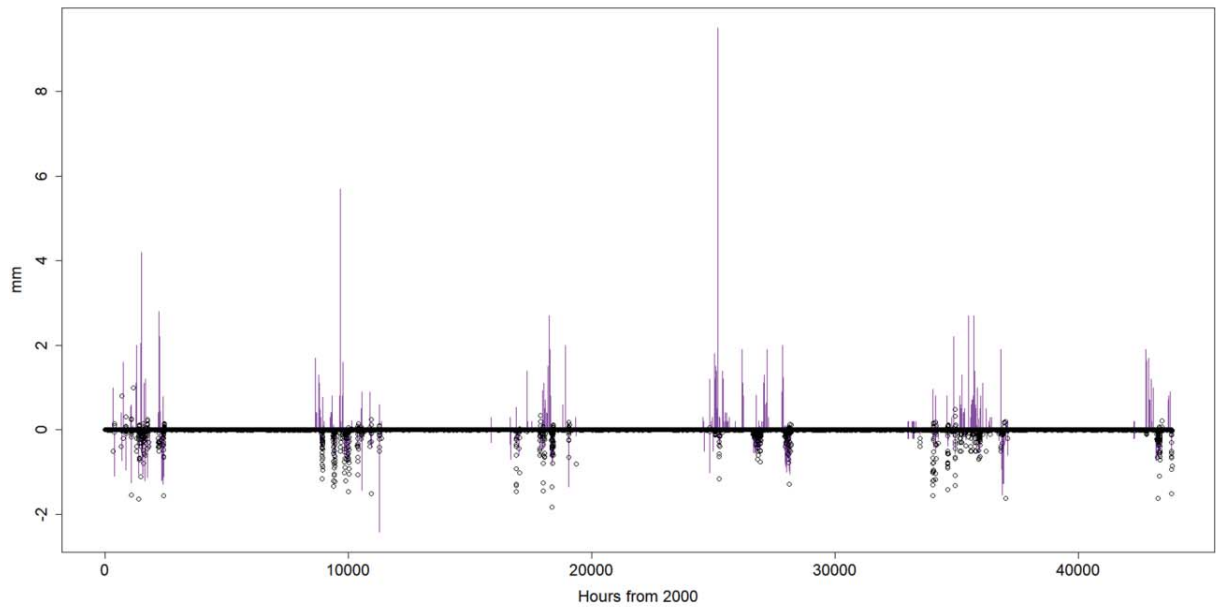


*Figure 37 Periods where water balance is negative (black). Corresponding periods where change in SWE is large (purple). 0 hours is January 1<sup>st</sup> 2000.*



# Conclusion

## 5.1. Aim and research objectives

The main goal of this thesis was to apply a rainfall-runoff model of high temporal resolution on an arable catchment to better understand runoff patterns and help mitigation in the future. The Distance Distribution Dynamics (DDD) model simulates runoff at a temporal resolution of 1h on the arable catchment Skuterud with acceptable results: A Nash-Sutcliffe Efficiency (NSE) and Kling-Gupta Efficiency (KGE) criterion of more than 0.50 for both calibration and validation period. Model scenarios with and without artificial drainage as river network in the distance distribution pre-processing were compared. The conclusion is that runoff simulation is better with artificial drainage network acting as river network. The main effect of altering the distance distribution is slower subsurface celerities, which results in better runoff simulation and flood peak estimation. Three different approaches to recession analysis were compared. Sources of error in the original recession method include sensitivity at low flow and high variability in celerity estimation for different season. Possible explanations could be, but is not limited to, inaccuracies in measurements at high temporal resolution during low flow, hysteresis and/or changing soil characteristics for different seasons. The altered methods improved results but did not solve the problem completely as none proved to be time invariant at 1h temporal resolution. Compared to previous studies the DDD simulate 1h runoff at similarly to DRAINMOD, COUP, INCA, HBV and SWAT do at 24-hour simulation. The use of a parsimonious rainfall-runoff model is thus applicable for agricultural catchments and high temporal resolution.

## 5.2. Reflections and further studies

The result of this study shows that rainfall-runoff modelling on arable catchment using a parsimonious model yields acceptable results. Many calibrated parameters are not needed to obtain accurate simulations. Further, simple physically based models are robust, usable for ungauged basins and for future modelling. They can, however, be inclined to provide an inaccurate representation of reality with negative runoff, low evapotranspiration and negative water balance.

The use of high temporal resolution modelling helps understand the diurnal fluctuation in runoff patterns and what is causing it. This is especially important for flood forecasters, and for mitigation strategies that aim to minimise anthropogenic impact on our water bodies.

Further testing and improvement of the DDD model for other arable catchments is needed. A sensitivity analysis of different parameters in model to investigate what parameters cause the greatest uncertainty and have the biggest effect on model result could also be constructive. One solution to the high celerities for low storage problem could be to use infiltration rates instead of recession rates or only conduct recession analysis at night. A solution to the problem of high variation in recession characteristics could be to assign different characteristics according to seasons, or sorption and desorption period, in the model. The use of scaled values from 24-hour time series might solve the problem related to gauge limitation at high temporal resolution during low flow.

# References

- Arnold, J. G., Srinivasan, R., Muttiah, R. S. & Williams, J. R. (1998). Large Area Hydrologic Modeling and Assessment Part I: Model Development. *Journal of the American Water Resources Association (JAWRA)*, Volume 34 (Issue 1). doi: 10.1111/j.1752-1688.1998.tb05961.x.
- Bechmann, M. & Deelstra, J. (2013). *Agriculture and Environment - Long Term Monitoring in Norway*. Trondheim: Akademika Publishing. p. 9-10, 12.
- Beven, K. (2012). *Rainfall-Runoff Modelling: The Primer*. Second edition ed.: John Wiley & Sons, Ltd. p. 16-17.
- BIOKLIM. (2014a). *Nedbør, fordampning og luftfuktighet*. nmbu.no. Available at: <https://www.nmbu.no/fakultet/realtek/laboratorier/bioklim/maleinstrumenter/nedbor> (accessed: 28.02).
- BIOKLIM. (2014b). *Temperatur*. nmbu.no. Available at: <https://www.nmbu.no/fakultet/realtek/laboratorier/bioklim/maleinstrumenter/temperatur> (accessed: 29.02).
- BIOKLIM. (2017). *Meteorologiske data for Ås - BIOKLIM*. Available at: <https://www.nmbu.no/fakultet/realtek/laboratorier/bioklim>.
- Blann, K. L., Anderson, J. L., Sands, G. R. & Vondracek, B. (2009). Effects of Agricultural Drainage on Aquatic Ecosystems: A Review. *Critical Reviews in Environmental Science and Technology*, 39 (11): 909-1001. doi: 10.1080/10643380801977966.
- Brodie, R. & Hostetler, S. (2005). *A review of techniques for analysing baseflow from stream hydrographs*. Proceedings of the NZHS-IAH-NZSSS 2005 conference: Auckland New Zealand.
- Cerdà, A. (1996). Seasonal variability of infiltration rates under contrasting slope conditions in southeast Spain. *Geoderma*, Volume 69 (Issues 3–4): Pages 217-232. doi: 10.1016/0016-7061(95)00062-3.
- Constantz, J. & Murphy, F. (1991). The temperature dependence of ponded infiltration under isothermal conditions. *Journal of Hydrology*, Volume 122 (Issues 1–4): Pages 119-128. doi: 10.1016/0022-1694(91)90175-H.
- Deelstra, J., Kværnø, S. H., Skjævdal, R., Vandsemb, S., Eggestad, H. O. & Ludvigsen, G. H. (2005). *A general description of the Skuterud catchment*: Norwegian Centre for Soil and Environmental Research.

- Deelstra, J. & Iital, A. (2006). The flashiness index and transport/retention of nutrients and suspended solids. . *In NJF Seminar 373* (p. 62).
- Deelstra, J. & Iital, A. (2008). The use of the flashiness index as a possible indicator for nutrient loss prediction in agricultural catchments. *Boreal Environment Research*, 13: 209-221.
- Deelstra, J., Eggestad, H., Iital, A., Jansons, V. & Barkved, L. (2010). Time resolution and hydrological characteristics in agricultural catchments. *Status and Perspectives of Hydrology in Small Basins - IAHS Red books series*. ( 336): 138-143.
- Deelstra, J., Øygarden, L., BlankenBerg, A. B. & Eggestad, H. O. (2011). Climate change and runoff from agricultural catchments in Norway. *International Journal of Climate Change Strategies and Management*, Vol. 3 (Issue: 4): pp.345-360. doi: 10.1108/17568691111175641.
- Deelstra, J., Ital, A., Grønsten, H., Paruch, A. . (2008). *Nutrient load assessment from agriculture in the Leningrad Oblast*. TemaNord.
- Dingman, S. L. (2015). *Physical hydrology*. Long Grove, Illinois: Waveland press, Inc. p. 505-508, 595-604.
- Dooge, J. C. I. (1959). A General Theory of the Unit Hydrograph. *Journal of Geophysical Research*, 64 (2): 241-256.
- Esri. (2019). *ArcGIS pro*. Available at: <https://pro.arcgis.com/en/pro-app/>.
- Farkas, C., Kværnø, S., Engebretsen, A., Barneveld, R. & Deelstra, J. (2016). Applying profile- and catchment based mathematical models for evaluating the run-off from Nordic catchment. *J. Hydrol. Hydromech*, 64 (3): 218-225. doi: 10.1515/john-2016-0022.
- Fikse, A. N. (2016). *Modelling water infiltration and transport in an agricultural compacted soil*. Brage Bibsys: Norwegian University of Life Sciences.
- Foundation, T. R. (2019). *The R Project for Statistical Computing*. Available at: <https://www.r-project.org/>.
- Geonorge. (2018). *Kartkatalogen*. Available at: <https://kartkatalog.geonorge.no/search>.
- Gramlich, A., Stoll, S., Stamm, C., Walter, T. & Prasuhn, V. (2018). Effects of artificial land drainage on hydrology, nutrient and pesticide fluxes from agricultural fields – A review. *Agriculture, Ecosystems & Environment*, Volume 266: Pages 84-99. doi: <https://doi.org/10.1016/j.agee.2018.04.005>.
- Gupta, H. V., Kling, H., Yilmaz, K. K. & Martinez, G. F. (2009). Decomposition of the mean squared error and NSE performance criteria: Implications for improving hydrological modelling. *Journal of Hydrology* 377: 80-91. doi: 10.1016/j.jhydrol.2009.08.003.
- Hauge, A., Kværnø, S. H., Deelstra, J. & Bechmann, M. (2011). *Dreneringsbehov i norsk landbruk – økonomi i grøftingen*.

- Hillel, D. (1998). *Environmental Soil Physics*. San Diego: Academic Press. An Imprint of Elsevier. p. 78.
- Jansson, P. & Karlberg, L. (2004). COUP manual - coupled heat and mass transfer model for soil-plant-atmosphere systems. *Technical Manual for the CoupModel*: 1-453.
- Jarritt, N. P. & Lawrence, D. S. L. (2006). Chapter 20: simulating fine sediment delivery in lowland catchments: model development and application of INCA-Sed. In P.N. Owens, A. J. C. E. (ed.) *Soil Erosion and Sediment Redistribution in River Catchments*: CAB International.
- JOVA. (2019). *The Norwegian Agricultural Environmental Monitoring Programme (JOVA)*. Available at: <https://www.nibio.no/en/subjects/environment/the-norwegian-agricultural-environmental-monitoring-programme-jova>.
- Kartverket. (2019). *Høydedata og terrengmodeller for landområdene*. Available at: <https://www.kartverket.no/data/Hoydedata-og-terrengmodeller/>.
- Kirchner, J. W. (2009). Catchments as simple dynamical systems: Catchment characterization, rainfall-runoff modeling, and doing hydrology backward. *Water Resources Research*, 45 (2). doi: 10.1029/2008wr006912.
- Klimaservicesenter, N. *Klimaframskrivninger*. Available at: [https://klimaservicesenter.no/faces/desktop/scenarios.xhtml?climateIndex=air\\_temperatur\\_e&period=Annual&scenario=RCP85&region=NO&mapInterval=2085](https://klimaservicesenter.no/faces/desktop/scenarios.xhtml?climateIndex=air_temperatur_e&period=Annual&scenario=RCP85&region=NO&mapInterval=2085) (accessed: 07.02).
- Lindström, G., Johansson, B., Persson, M., Gardelin, M. & Bergström, S. (1997). Development and test of the distributed HBV-96 hydrological model. *Journal of Hydrology*, Volume 201 (Issues 1–4): Pages 272-288. doi: 10.1016/S0022-1694(97)00041-3.
- Miller, J. D., Kim, H., Kjeldsen, T. R., Packman, J., Grebby, S. & Dearden, R. (2014). Assessing the impact of urbanization on storm runoff in a peri-urban catchment using historical change in impervious cover. *Journal of Hydrology*, 515: 59-70. doi: <https://doi.org/10.1016/j.jhydrol.2014.04.011>.
- Moriasi, D. N., Arnold, J. G., Liew, M. W. V., Bingner, R. L., Harmel, R. D. & Veith, T. L. (2007). Model evaluation guidelines for systematic quantification of accuracy in watershed simulations. *Transaction of the ASABE*, 50 (3): 885-900.
- Nash, J. E. & Sutcliffe, J. V. (1970). River flow forecasting through conceptual models. Part 1 - A discussion of principles. *Journal of Hydrology*, 10: 280-290.
- NIBIO. (2019). *Kilden: Kartdata: Kartverket, Geovekst og kommunene*. Available at: [https://kilden.nibio.no/?lang=nb&topic=arealinformasjon&bgLayer=graatone\\_cache](https://kilden.nibio.no/?lang=nb&topic=arealinformasjon&bgLayer=graatone_cache).
- Nyborg, Å. A. (2008). *Jordsmonn utviklet i marin leire i Østfold - egenskaper, opptreden og utbredelse*. Oppdragsrapport fra Skog og landskap.

- Priestley, C. H. B. & Taylor, R. J. (1972). On the Assessment of Surface Heat Flux and Evaporation Using Large-Scale Parameters. *Monthly Weather Review*, 100 (2): 81-92. doi: 10.1175/1520-0493(1972)100<0081:Otaosh>2.3.Co;2.
- Ramirez, J. A. (2000). Prediction and modeling of flood hydrology and hydraulics. In Wohl, E. (ed.) *Inland Flood Hazards: Human, Riparian and Aquatic Communities* Cambridge University Press.
- Ritter, A. & Muñoz-Carpena, R. (2013). Performance evaluation of hydrological models: Statistical significance for reducing subjectivity in goodness-of-fit assessment. *Journal of Hydrology* (480): 33-45.
- Robinson, M., Ryder, E. L. & Ward, R. C. (1985). Influence on streamflow of field drainage in a small agricultural catchment. *Agricultural Water Management*, Volume 10 (Issue 2): Pages 145-158,. doi: 10.1016/0378-3774(85)90003-4.
- Romarheim, A. T. & Riise, G. (2009). Development of cyanobacteria in Årungen VANN (04): 384-393.
- RStudio, I. (2019). *R Studio - Open Source enterprise-ready professional software for R*. Available at: <https://www.rstudio.com/>.
- Rupp, D. E. & Selker, J. S. (2006). Information, artifacts, and noise in  $dQ/dt-Q$  recession analysis. *Advances in Water Resources*, Volume 29 (Issue 2): Pages 154-160. doi: 10.1016/j.advwatres.2005.03.019.
- Sherman, L. K. (1932). Streamflow from rainfall by unit-graph method. *Engineering News Record* 108: 501-505.
- Sitterson, J., Knightes, C., Parmar, R., Wolfe, K., Muche, M. & Avant, B. (2017). *An Overview of Rainfall-Runoff Model Types*. . Washington, DC.: U.S. Environmental Protection Agency.
- Skaggs, R. W., Youssef, M. A. & Chescheir, G. M. (2012). DRAINMOD: Model Use, Calibration, and Validation. *Transactions of the ASABE*, 55 (4): 1509-1522. doi: 10.13031/2013.42259.
- Skaugen, T. & Onof, C. (2014). A rainfall-runoff model parameterized from GIS and runoff data. *Hydrol. Process.*, 28: 4529-4542. doi: 10.1002/hyp.9968.
- Skaugen, T., Peerebom, I. O. & Nilsson, A. (2015). Use of a parsimonious rainfall-run-off model for predicting hydrological response in ungauged basins. *Hydrol. Process.*, 29: 1999-2013. doi: 10.1002/hyp.10315.
- Skaugen, T. & Saloranta, T. (2015). *Simplified energy-balance snowmelt modelling*: NVE.
- Skaugen, T. & Mengistu, Z. (2016). Estimating catchment scale groundwater dynamics from recession analysis - enhanced constraining og hydrological models. *Hydrol. Earth Syst. Sci*, 20: 4963-4981. doi: 10.5194/hess-20-4963-2016.

- Skaugen, T. & Weltzien, I. H. (2016). A model for the spatial distribution of snow water equivalent parameterized from the spatial variability of precipitation. *The Cryosphere*, 10: 1947-1963. doi: 10.5194/tc-10-1947-2016.
- Skaugen, T. (2018). *The DDD (Distance Distribution Dynamics) model - a parameter parsimonious rainfall runoff model. Basic principles and ideas (Powerpoint slides)*. Presentation in VANN300: Water Pollution I, NMBU.
- Slawinski, C. (2011). *Hysteresis in Soil*. In Gliński J., H. J., Lipiec J. (ed.). Encyclopedia of Agrophysics. Encyclopedia of Earth Sciences Series. Dordrecht: Springer.
- Smol, J. P. (2008). *Pollution of Lakes and Rivers: A Paleoenvironmental Perspective*: Wiley-Blackwell.
- Stoelzle, M., Stahl, K. & Weiler, M. (2013). Are streamflow recession characteristics really characteristic? . *Hydrol. Earth Syst. Sci*, 17: 817-828. doi: 10.5194/hess-17-817-2013.
- Subramanya, K. (2013). *Engineering hydrology* New Dehli: McGraw Hill Education (India) Private Limited. p. 235-241.
- Tallaksen, L. M. (1995). A review of baseflow recession analysis. *Journal of Hydrology*, 165: 349-370.
- Union, E. P. a. t. C. o. t. E. (2000). *Directive 2000/60/EC of the European Parliament and of the Council of 23 October 2000: Establishing a framework for Community action in the field of water policy*. Official Journal of the European Communities.
- Vagstad, N. & Bechmann, M. (2013). Long term monitoring data and its role in society decision making. In Bechmann, M. & Deelstra, J. (eds) *Agriculture and Environment - Long Term Monitoring in Norway*. Trondheim: Akademika Publisher.
- Weisman, R. N. (1977). The Effect Of Evapotranspiration on Streamflow Recession *Hydrological Sciences Bulletin*,, 22 (3): 371-377. doi: DOI: 10.1080/02626667709491731.
- Zambrano-Bigiarini, M. & Rojas, R. (2013). A model-independent Particle Swarm Optimisation software for model calibration. *Environmental Modelling & Software*, Volume 43: 5-25. doi: 10.1016/j.envsoft.2013.01.004.
- Zambrano-Bigiarini, M. (2017a). *hydroGOF: Goodness-of-fit functions for comparison of simulated and observed hydrological time series*. Unpublished manuscript.
- Zambrano-Bigiarini, M. (2017b). *hydroTSM: Time Series Management, Analysis and Interpolation for Hydrological Modelling*. doi: 10.5281/zenodo.839864.
- Øygarden, L. & Botterweg, P. (1998). *Measuring Runoff and Nutrient Losses from Agricultural Land in Nordic Countries: A Guideline for Good Measurement Practices*: Nordic Council of Ministers.







**Norges miljø- og biovitenskapelige universitet**  
Noregs miljø- og biovitenskapelige universitet  
Norwegian University of Life Sciences

Postboks 5003  
NO-1432 Ås  
Norway